Received: 23 October 2024 | Revised: 29 September 2025 | Accepted: 3 October 2025

DOI: 10.1002/suco.70365

ARTICLE

fib CEB-FIP WILEY

Notch depth-dependent flexural behavior of high-performance fiber-reinforced concrete under static and cyclic loading

Kha-Ky Lam[1] | **Duy-Liem Nguyen**[1] | **H. T. Tai Nguyen**[1] | **Kien Le-Trung**[1] | **Ngoc-Thanh Tran**[2] | **Huy-Viet Le**[3]

[1]Faculty of Civil Engineering, Ho Chi Minh City University of Technology and Education, Ho Chi Minh City, Vietnam

[2]Institute of Civil Engineering, Ho Chi Minh City University of Transport, Ho Chi Minh City, Vietnam

[3]Faculty of Civil Engineering, Hanoi University of Mining and Geology, Ha Noi, Vietnam

Correspondence
Duy-Liem Nguyen, Faculty of Civil Engineering, Ho Chi Minh City University of Technology and Education, No. 01 Vo Van Ngan St, Thu Duc Ward, Ho Chi Minh City, Vietnam.
Email: liemnd@hcmute.edu.vn

Funding information
Vietnam National Foundation for Science and Technology Development, Grant/Award Number: 107.01-2021.69

Abstract

This study aims to explore notch depth-dependent flexural behavior of high-performance fiber-reinforced concrete (HPFRC) under static and cyclic flexural load. All specimens with their size of 40 × 40 × 160 mm (width × depth × full length) and span of 120 mm were tested under three-point bending load. Three HPFRC types included: no fiber (HPFRC0), 1.0 vol% long hooked fiber blended with 0.5 vol% short smooth fiber (HPFRC1), and 0.5 vol% long hooked fiber blended with 1.0 vol% short smooth fiber (HPFRC2). Three notch depths of 5, 10, and 15 mm were studied for each HPFRC type. Under static load, there were clear reductions in load-carrying capacity, deflection capacity, critical stress intensity factor, and critical energy release rate, but there was an increase in elastic modulus and crack mouth opening displacement as the notch depth increased from 5 to 15 mm, regardless of the HPFRC type. Generally, the order of the HPFRC type in terms of static flexural resistance was HPFRC0 < HPFRC2 < HPFRC1. Under fatigue load, at the high fatigue stress ratio of more than 0.6, the endurance limits of the HPFRCs reduced with increasing notch depth. Besides, the HPFRCs can be categorized as high-cycle fatigue materials since their cycle number changed from 100 to 1,000,000.

KEYWORDS

crack mouth opening displacement, critical energy release rate, critical stress intensity factor, endurance limit, notch-to-depth ratio

1 | INTRODUCTION

There has been urgent demand to improve the durability and resistance of civil and military infrastructure under serious environmental and mechanical loadings. High-performance fiber-reinforced concrete (HPFRC) is considered one of the most promising materials for meeting the demand.[1,2] This is because HPFRC has been characterized by its superior mechanical properties and durability due to its multi-microcrack accompanied work hardening process and high microstructure densification.[3] The superior mechanical properties of HPFRCs can be summarized as follows: great compressive and tensile strength, and high energy absorption.[4–6] In addition to their superior mechanical properties, HPFRCs also demonstrate smart characters, such as self-damage-sensing,[7–10] self-compacting,[11,12] and self-crack-healing.[13–15]

 © 2025 International Federation for Structural Concrete.

Cracks are a popular problem in any concrete construction, involving crack nucleation, propagation, and detection.[16] Therefore, understanding the foundation of cracks, conducting preventive measures during construction and applying appropriate treatment methods are critically important.[17] The stress intensity factor (K_{IC}) indicates a material's resistance to crack initiation and propagation under mode I fracture.[18] The mechanism of crack propagation is linked to an inelastic zone formed from pre-existing flaws in materials.[19] Numerous studies have focused on the fracture behavior of concrete using notched specimens.[20–22] Jiao et al.[20] investigated the effect of notch-to-depth (N/D) ratios from 0.2 to 0.5 on the fracture behavior of ultra-high-performance glass sand concrete under four-point bending (4 PB). The results showed that as the N/D increased, the peak load decreased: the flexural strength dropped by 14.77%, 16.08%, and 10.06% for N/D ratios of 0.3, 0.4, and 0.5, respectively, compared with N/D of 0.2. Yin et al.[21] studied the influence of changing initial N/D ratios, from 0.2 to 0.6, on the fracture properties of normal concrete under 4 PB. They found that the peak load decreased as the initial notch depth increased from 0.2 to 0.6, while the critical crack mouth opening displacement increased with the notch depth. Qin et al.[22] explored the fracture behavior of steel-fiber-reinforced high-strength concrete using notched concrete specimens with their size of 100 mm × 100 mm × 515 mm and N/D ratios of 0.4 and 0.5. They concluded that the critical stress intensity factor (K_{IC}) of the concretes was not significantly influenced with different N/D ratios, although it slightly decreased with increasing N/D ratio. Some recent studies have focused on behavior of fiber-reinforced concretes under various loadings using finite element modeling (FEM).[23–25] Specifically, Vandecruys et al.[23] conducted a sectional analysis of the cyclic response of steel fiber reinforced concrete, and they stated that the analysis results showed good agreement with the theoretical S–N curve. Zhu et al.[24] presented an experimental and numerical study on T-shape UHPFRC beams strengthened with high-strength bars. The authors reported that the bending stiffness and strength of the beams increased as the reinforcement ratio increased. Additionally, the result from numerical analysis using ABAQUS was consistent with the test results. Nasiri et al.[25] explored the flexural and shear behavior of ultra high-performance fiber-reinforced concrete beams strengthened with steel fiber and high-strength bars under cyclic loading by FEM. The numerical results indicated that the beams demonstrated stable flexural performance prior to failure. However, there is still limited research on the fracture properties of notched specimens using HPFRC. Furthermore, information on fatigue behaviors of HPFRC specimens with different notch depth is also questionable. This really becomes a research gap required further study for better understanding.

This above situation was the authors' motivation to conduct an experimental study combined with an analytical analysis performed in this paper, which focuses on the notch-dependent flexural behavior of HPFRC specimens under static and repeated loading. The main objectives of this investigation are as follows: (1) to explore the effect of notch-to-depth ratios on mechanical properties of notched HPFRC specimens under static loading; (2) to investigate the fatigue flexural response of notched HPFRC specimens. To achieve these objectives, a combination of experimental tests and analytical analysis was conducted to investigate the flexural responses of notched HPFRC specimens under both static and cyclic loading. Compared with the reviewed studies, this research work mainly focused on the static fracture parameters of notched HPFRC specimens, in addition to the comparative fatigue performance regarding various concrete types. The findings of this study aim to partially address the research gap mentioned above, as well as offer new insights into the notch depth-dependent flexural behavior of HPFRC.

2 | FLEXURAL BEHAVIORS OF NOTCHED HPFRC SPECIMENS UNDER STATIC AND CYCLIC LOADING

2.1 | Static behaviors of HPFRCs using notched specimen

Under static flexural loading, plain HPFRC without fibers always demonstrates deflection-softening behavior.[26–29] With the aid of reinforcing fibers, HPFRC can exhibit either deflection-softening or deflection-hardening behavior, depending on the content and other characteristics of the fibers.[30–32] Figure 1 shows the static flexural

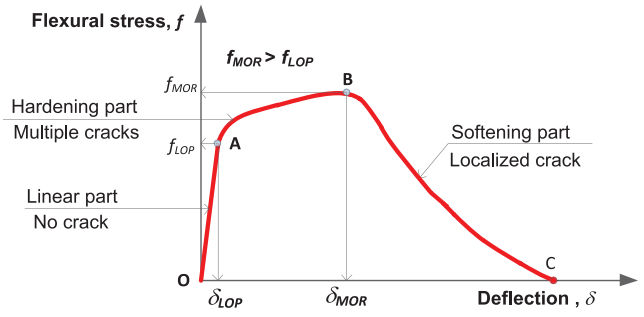


FIGURE 1 A typical flexural stress versus deflection behaviors of HPFRCs under static loading.

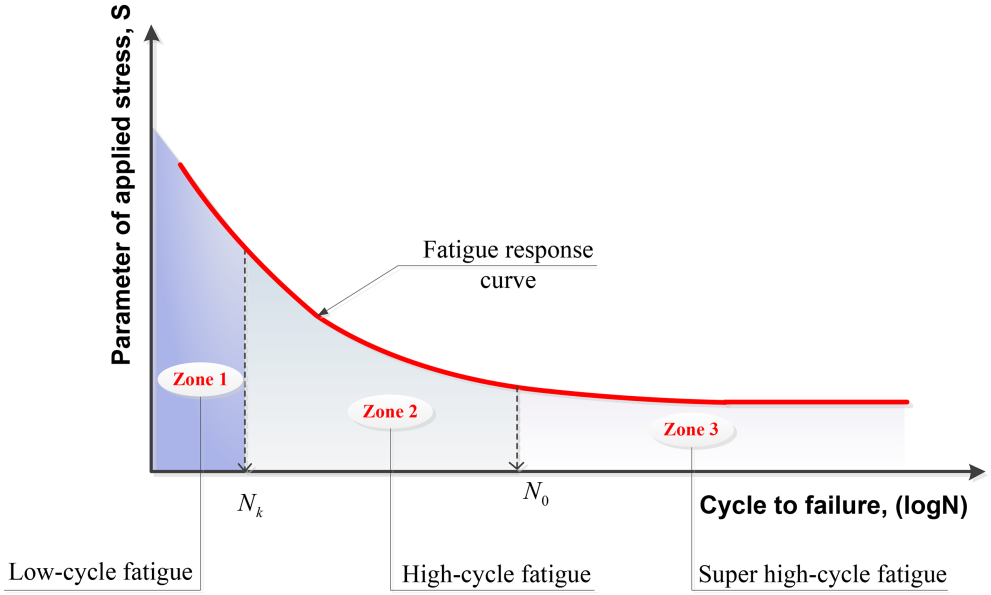


FIGURE 2 A typical fatigue response cure of the HPFRCs.

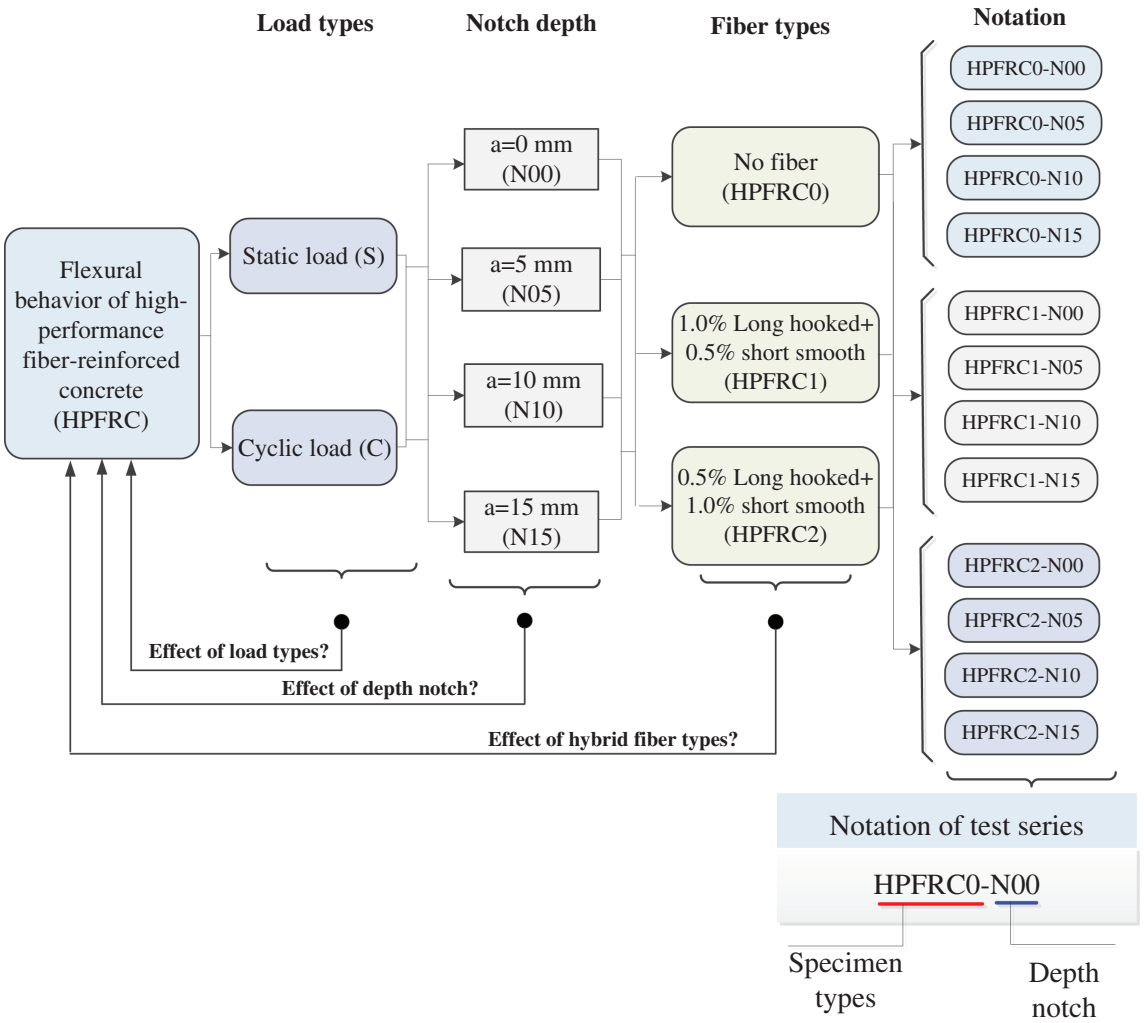


FIGURE 3 Flowchart of the experimental program.

stress versus deflection behaviors of HPFRC. In Figure 1, point $A(f_{LOP}, \delta_{LOP})$ is defined as the limit of proportionality (LOP), while point $B(f_{MOR}, \delta_{MOR})$ is defined as the modulus of rupture (MOR). The deflection-hardening behavior of HPFRC occurs when $f_{MOR} \geq f_{LOP}$.[33,34] Under 3 PB loading, the relationship between the applied load, moment, and flexural strength at MOR can be determined using Equation (1). Meanwhile, the elastic modulus (E) of the notched specimen can be indirectly computed using Equation (2),[35] where it is assumed that both moment and shear contribute to midspan deflection.

$$f_{MOR} = \frac{6M_{max}}{b(h-a)^2} = \frac{3P_{max}L}{2b(h-a)^2}, \quad (1)$$

$$E = \frac{f_{MOR}L^2}{6\delta_{MOR}(h-a)}\left(1 + \frac{2(1+\nu)}{\psi}\left(\frac{h-a}{L}\right)^2\right) = \frac{f_{MOR}L^2}{6\delta_{MOR}(h-a)}\left(1 + 2.817\left(\frac{h-a}{L}\right)^2\right), \quad (2)$$

where M_{max}, P_{max} are the maximum moment and maximum applied load, respectively; The tested specimens have span length of $L = 120$ mm, section width of $b = 40$ mm, section depth of $h = 40$ mm, notch depth of $a = 0$, 5, 10, and 15 mm; Poisson's ratio of $\nu = 0.2$, and shear factor of $\psi = 1/1.5$ for rectangular section. The specimen size was selected to match the 30 kN load capacity of the dynamic testing system (DTS) machine. With better equipment, all specimen edges should be at least three times the fiber length to ensure a uniform distribution of fibers within the concrete mixture.[36]

2.2 | Fatigue behaviors of HPFRCs using notched specimen

Fatigue behavior is often performed using S–N Wöhler curve,[37] as illustrated in Figure 2. In this figure, the horizontal axis represents the number of load cycles (N) leading to material failure, while the vertical axis (S) represents the parameter of applied stress with different forms according to maximum stress (f_{max}) and minimum tress, for example, $S = \Delta f_{max} = f_{max} - f_{min}$,[38,39] $S = (f_{max} - f_{min}) \times 0.5$,[40,41] $S = f_{max}/f_{MOR}$,[42,43] and $S = \Delta f_{max}/f_{MOR}$.[38,39] The choice of applied stress form depends on the objectives of the study. Regarding Figure 2, the categorization of structures based on the

TABLE 1 Matrix composition of HPFRCs by weight ratio and compressive strength.

Cement	Silica fume	Silica sand	Fly ash	Superplasticizer	Water	Compressive strength f'_c
0.80	0.07	1.00	0.20	0.04	0.26	72

TABLE 2 Chemical and physical characteristics of cement, silica fume, and fly ash.

Characteristics	Composition	Cement (Insee, PCB 40)	Silica fume	Fly ash
Chemical properties	SiO_2 (%)	20.60	95.38	56.25
	CaO (%)	62.6	0.13	
	Al_2O_3 (%)	5.10	0.20	20.04
	MgO (%)	3.00	0.37	1.30
	Fe_2O_3 (%)	3.20	0.0063	3.48
	SO_3 (%)	3.60	—	0.58
	$K_2O + Na_2O$ (%)	1.40	1.81	1.02
	C (%)	—	0.007	—
	Loss on ignition (%)	0.30	3,859	9.52
Physical properties	Fineness (m^2/kg)	348	20,000	289
	Specific gravity (g/cm^3)	3.15	2.24	2.41

TABLE 3 Fiber properties used in this study.

Fiber types	Diameter, d_f (mm)	Length, L_f (mm)	Aspect ratio (L/d)	Density (g/cm^3)	Tensile strength (MPa)
Long hooked	0.5	35	70	7.9	>1200
Short smooth	0.2	13	65	7.9	>2500

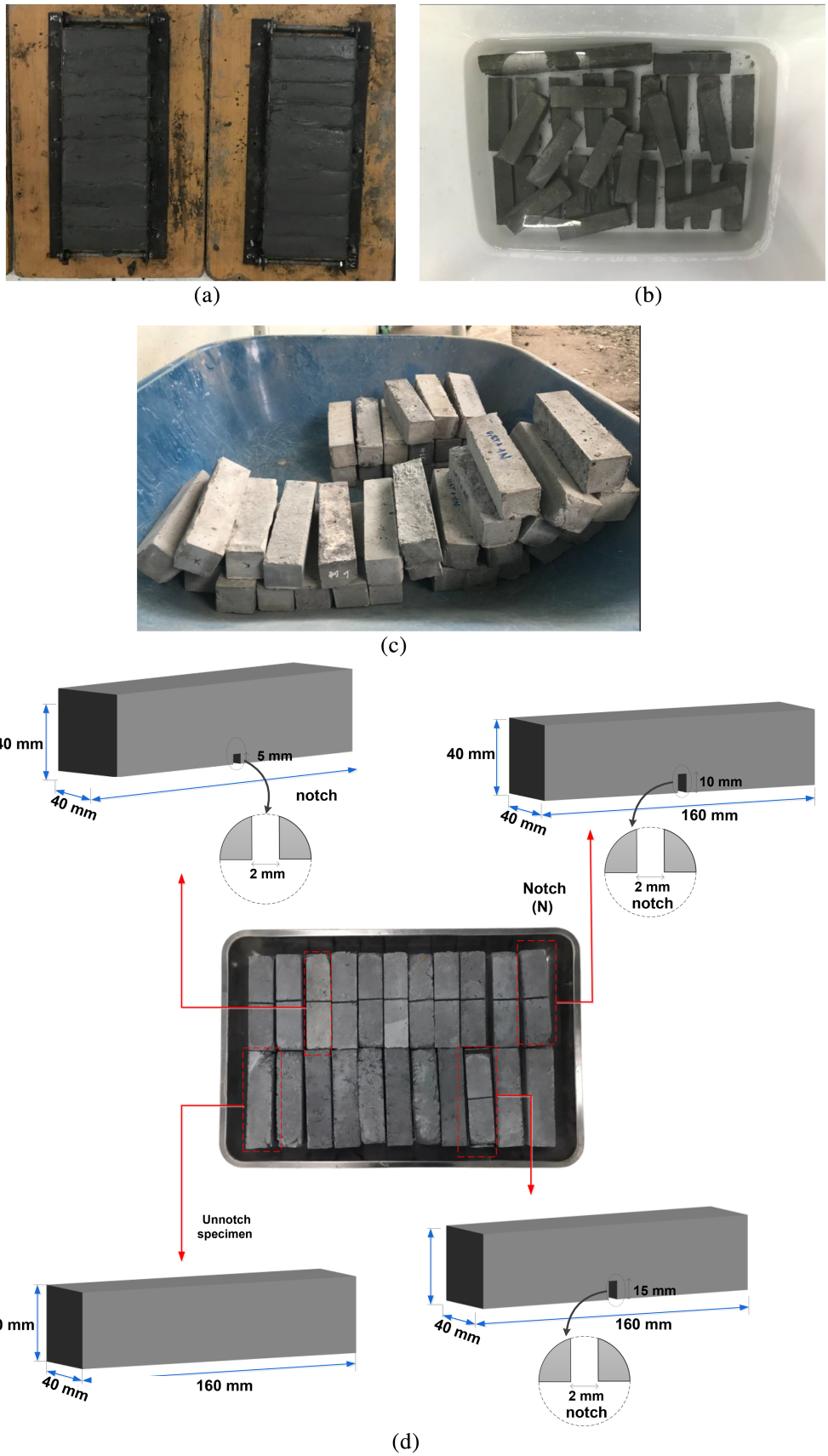


FIGURE 4 Preparation of flexural specimen HPFRCs. (a) Casting specimen. (b) Curing specimen in water. (c) Specimen after curing in water. (d) Detailed dimension of flexural specimen (unit: mm)

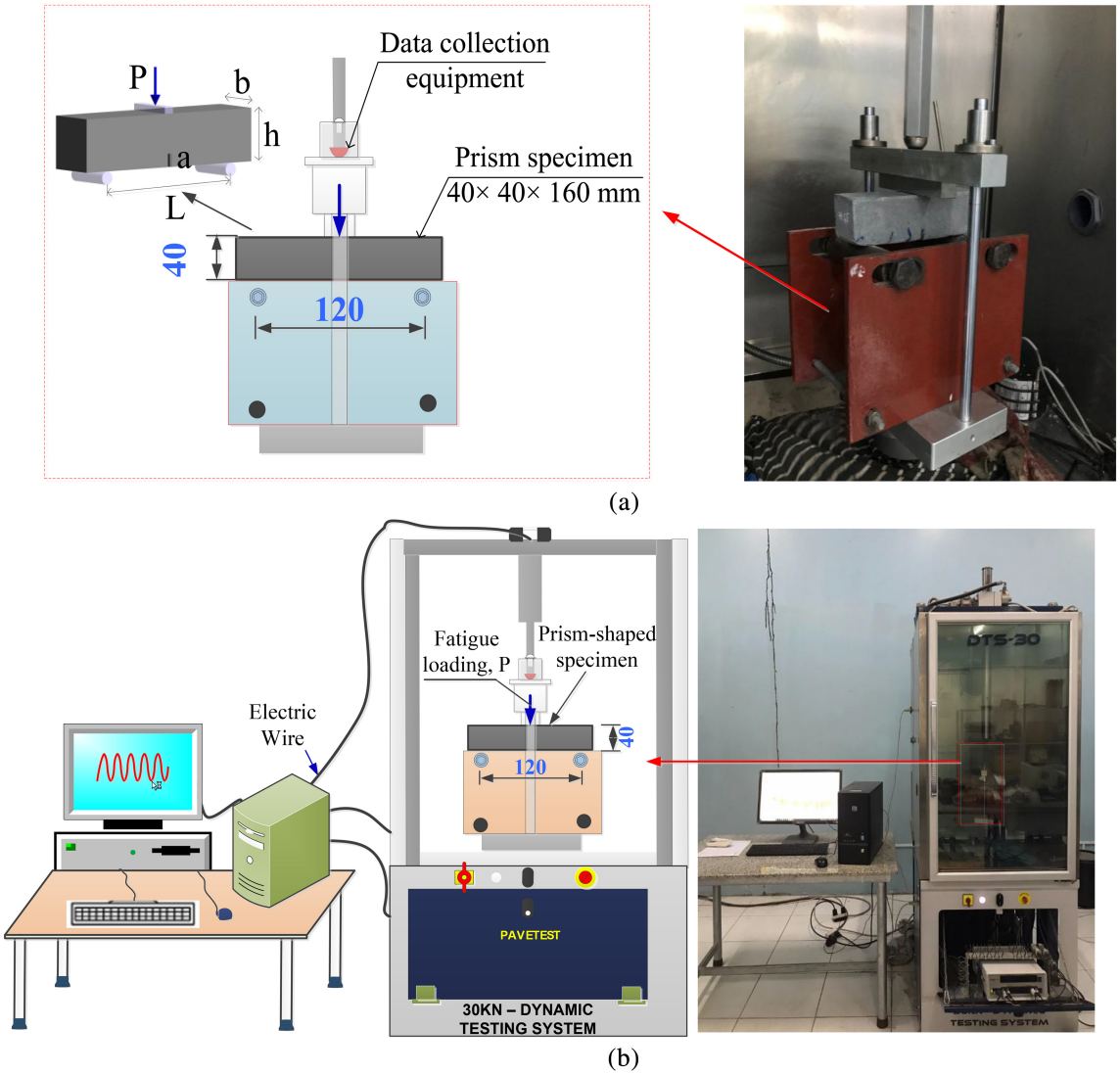


FIGURE 5 Detail of experimental system. (a) Flexural test under static loading. (b) Flexural test under cyclic loading.

typical number of cycles to failure comprises of three zones: low-cycle fatigue (Zone 1, $N \leq 100$), high-cycle fatigue (Zone 2, $100 \leq N \leq 1{,}000{,}000$), and super high-cycle fatigue (Zone 3, $N \geq 1{,}000{,}000$).[44]

3 | EXPERIMENTAL PROGRAM

Figure 3 shows the flowchart of the experimental program for this investigation. This study examines four levels of notch depth designed at the midspan of the specimen: 0 mm (named N00 series), 5 mm (named N05 series), 10 mm (named N10 series), and 15 mm (named N15 series). The notch-to-depth ratios in this study were kept below 0.4 to minimize their influence on stable crack growth.[45] The series of flexural HPFRC specimens

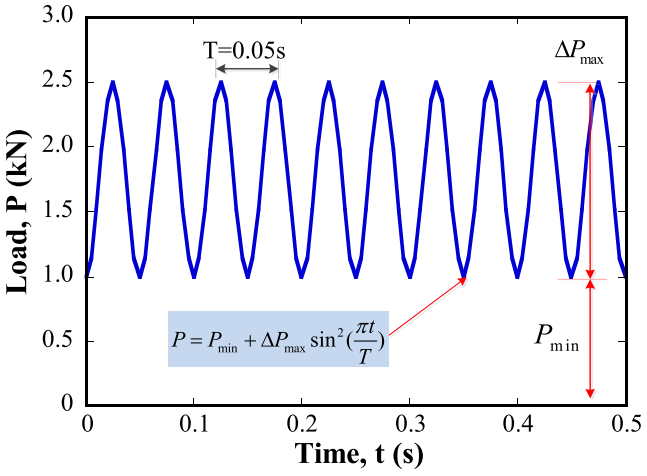


FIGURE 6 General cyclic loading used in flexural fatigue test.

are reinforced with different hybrid fibers, as follows: HPFRC0 (no fiber), HPFRC1 (1.0% by volume hooked fiber blended with 0.5% by volume smooth fiber), and HPFRC2 (0.5% by volume hooked fiber blended with 1.0% by volume smooth fiber). The static and cyclic flexural behaviors of HPFRC0 without a notch have been discussed in Vuong et al.[39] To strengthen the credibility of the findings, the experimental tests are encouraged to combine numerical validation methods (e.g., FEM). This study has no numerical analysis, which limits the generalizability and theoretical validation of the test results. This problem should be considered in future investigations.

3.1 | Materials and specimen preparing

Table 1 presents the composition of the plain HPFRC matrix by weight ratio, which achieved an average compressive strength of 72 MPa based on three 150 × 300 mm cylindrical specimens tested at 28 days after water curing at room temperature. The components of the mortar matrix include silica sand, cement, fly ash, silica fume, water, and superplasticizer. The chemical and physical properties of fly ash, cement, and silica fume are presented in Table 2. Table 3 shows the properties of short smooth and long hooked fibers used in this investigation.

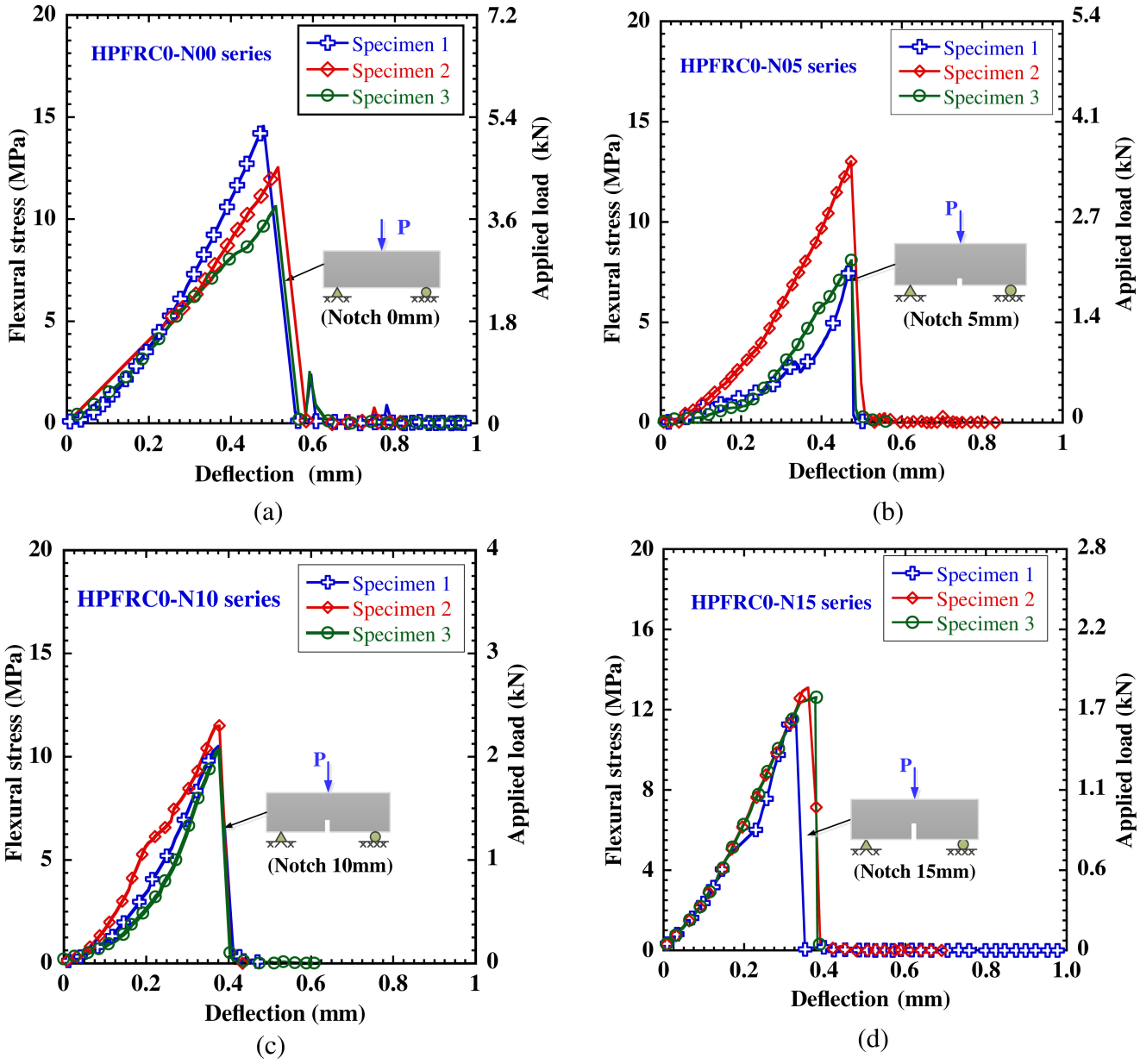


FIGURE 7 Flexural stress versus deflection of HPFRC0 with various depth notch under static loading. (a) HPFRC0-N00; (b) HPFRC0-N05; (c) HPFRC0-N10; (d) HFRC0-N15.

The HPFRCs specimens have dimensions of 40 × 40 × 160 mm, with notch depth located at the bottom mid-span. The study mixtures were prepared using a mixer with a capacity of 30 L. The mixing of componential materials was conducted at a room temperature of 25 ± 5°C and a humidity of 70 ± 5°C. The detail of mixing and curing can be referred to Vuong et al.[39] After 28 days of water curing, all specimens were tested at 30 days of age under both static and cyclic loads. The variability in material properties under static testing was addressed by averaging the results from three specimens for each mixture, thereby enhancing the transparency and reliability of the reported data. Accordingly, a total of 36 specimens were tested for the four different notch depths. In the cyclic loading test, four specimens from each HPFRC series were subjected to four different fatigue loading levels, resulting in a total of 48 specimens tested across the four notch depths. The corresponding standard deviations, standard errors, coefficients of variation, and error propagation are presented in the tables and figures in the following sections.

3.2 | Test setup

A DTS machine with a loading capacity of 30 kN was employed to conduct both static and fatigue bending tests, capable of delivering accurate loading waveforms

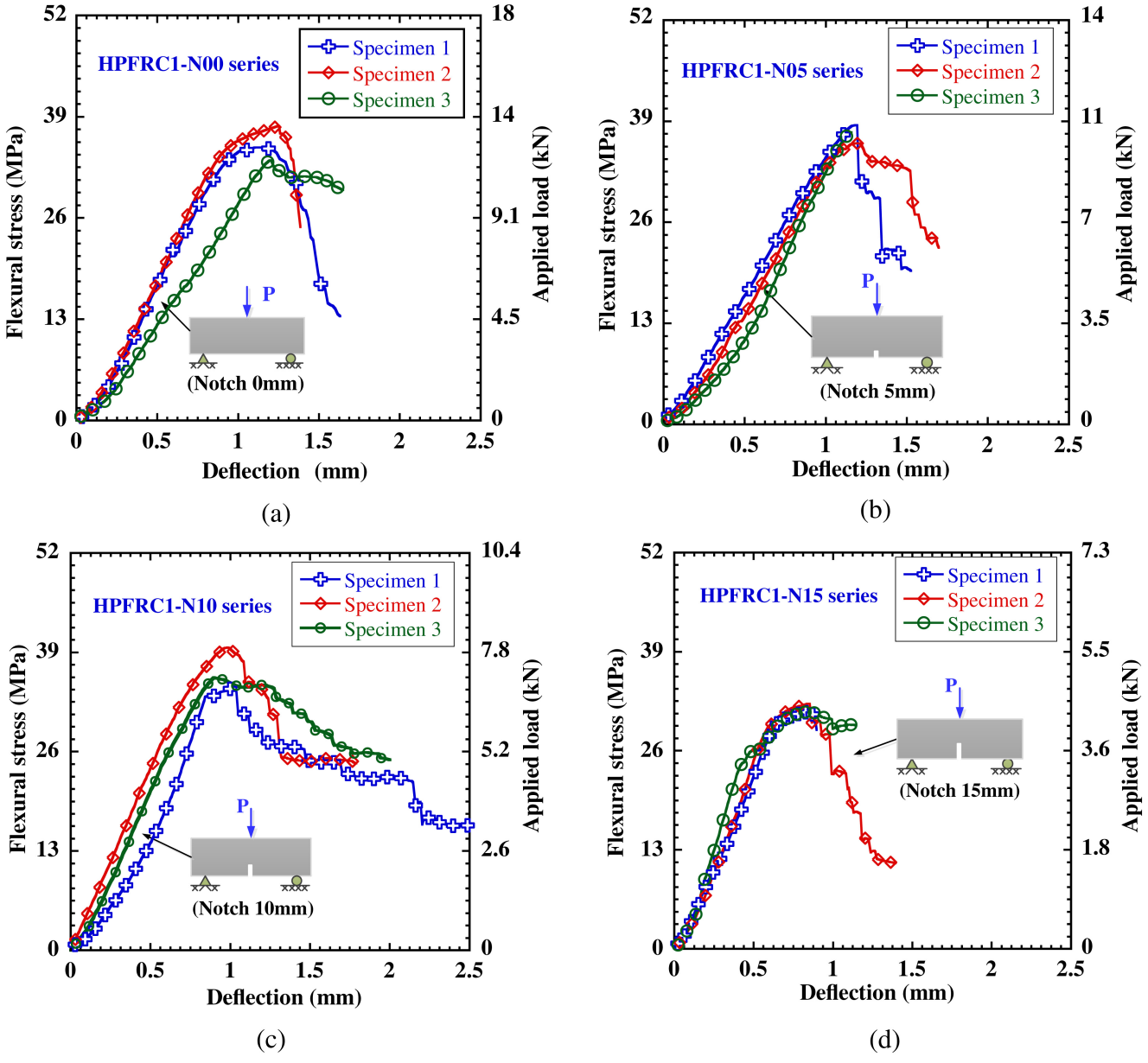


FIGURE 8 Flexural stress versus deflection of HPFRC1 with various notch depth under static loading. (a) HPFRC0-N00; (b) HPFRC0-N05; (c) HPFRC0-N10; (d) HFRC0-N15.

up to 100 Hz. The DTS is also equipped with a 100 mm actuator LVDT, a 2.2 kW hydraulic power supply, a maximum hydraulic pressure capacity of 21 MPa, and a 16-channel control and data acquisition system integrated with dedicated software. Figure 4 shows the test setup for the flexural specimen under static and cyclic loading. All specimens were tested in a 3 PB configuration with a span length of 120 mm, as displayed in Figure 5. The static loading was applied at a speed of 1 mm/min. During the loading process, the crosshead displacement at midspan was monitored, with data collected at a frequency of 1 Hz. The crosshead displacement was approximately considered as the midspan deflection. The applied load (P) was also recorded to derive flexural stress using Equation (1). All experiments were conducted under the same environmental conditions of $25 \pm 5°C$ and $70\% \pm 5\%$ relative humidity to ensure repeatability and minimize external influences.

$$P = P_{\min} + \Delta P_{\max} \sin^2\left(\frac{\pi t}{T}\right). \tag{3}$$

Equation (3) describes the sinusoidal form applied to the cyclic loads. The amplitude of cyclic load was applied to specimen as a percentage of the static load-bearing

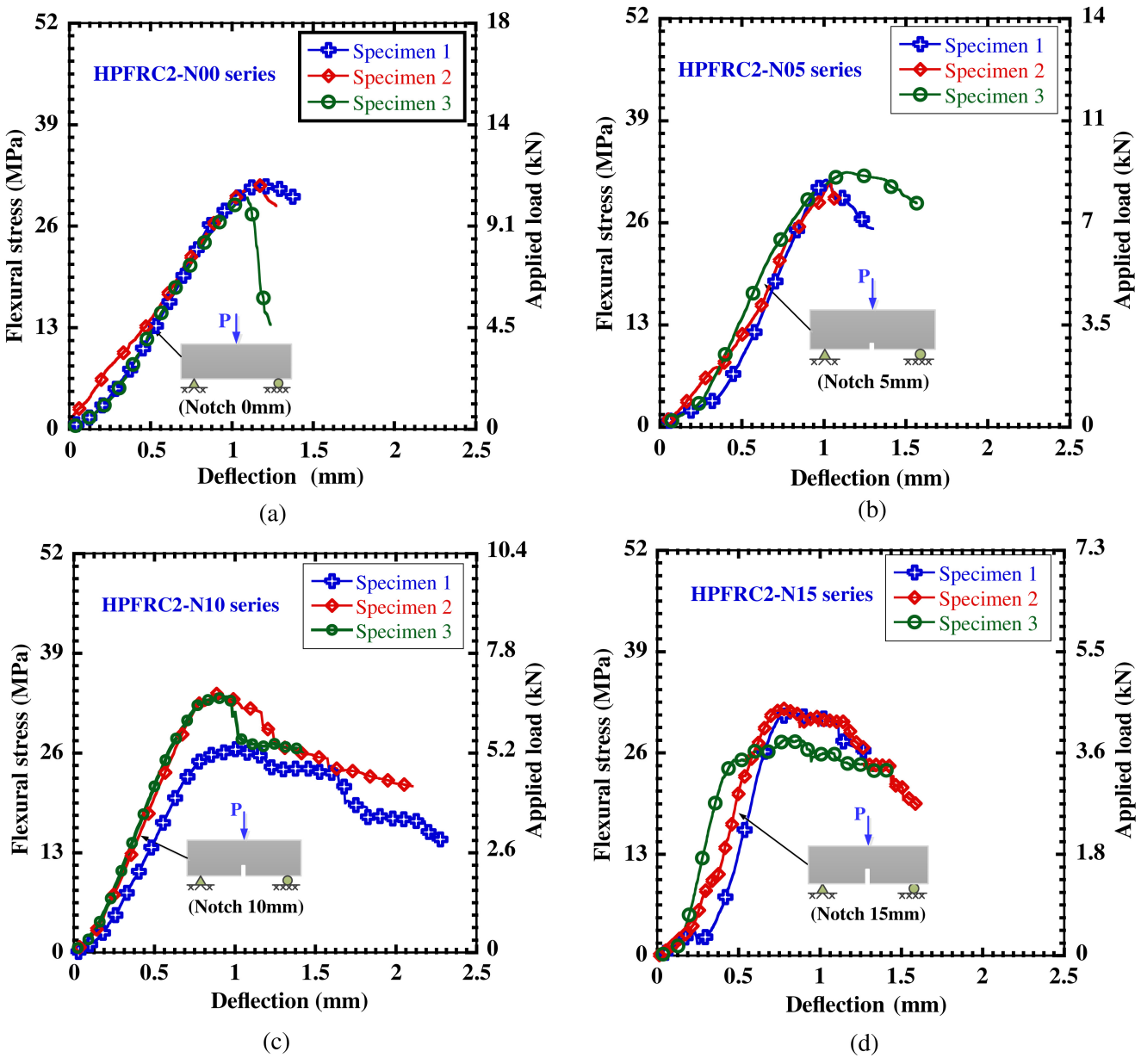


FIGURE 9 Flexural stress versus deflection of HPFRC2 with various notch depth under static loading. (a) HPFRC0-N00; (b) HPFRC0-N05; (c) HPFRC0-N10; (d) HFRC0-N15.

TABLE 4 Static flexural parameter of the investigated HPFRCs.

Test series		Force, P_{MOR}	Moment, M_{MOR}	Flexural strength, f_{MOR}	Deflection, δ_{MOR}	Elastic modulus, E
—	Ratio of $\alpha = \frac{a}{h}$	(kN)	(kN mm)	(MPa)	(mm)	(MPa)
HPFRC0 series [26]						
HPFRC0-N00	0.00	5.18	155.31	14.56	0.48	1924.74
		4.46	133.77	12.54	0.51	1866.76
		3.78	113.41	10.63	0.51	1642.22
Average value		**4.47**	**134.16**	**12.58**	**0.50**	**1811.24**
Standard deviations		*0.70*	*20.95*	*1.96*	*0.02*	*149.22*
Standard error		*0.40*	*12.10*	*1.13*	*0.01*	*86.15*
Coefficient of variation (%)		*15.66*	*15.62*	*15.58*	*4.00*	*8.24*
Error propagation (%)		*9.04*	*9.02*	*9.00*	*2.31*	*4.76*
HPFRC0-N05	0.125	2.30	69.06	8.46	0.47	1529.47
		3.55	106.43	13.03	0.47	2339.34
		2.57	77.14	9.45	0.48	1676.51
Average value		**2.81**	**84.21**	**10.31**	**0.47**	**1848.44**
Standard deviations		*0.66*	*19.66*	*2.41*	*0.09*	*431.44*
Standard error		*0.38*	*11.35*	*1.39*	*0.05*	*249.09*
Coefficient of variation (%)		*23.49*	*23.35*	*23.38*	*19.15*	*23.34*
Error propagation (%)		*13.56*	*13.48*	*13.50*	*11.06*	*13.48*
Standard error coefficient of variation	0.250	2.11	63.15	10.53	0.38	2629.98
		2.14	64.16	10.69	0.38	2664.99
		2.20	66.07	11.01	0.38	2747.96
Average value		**2.15**	**64.46**	**10.74**	**0.38**	**2680.98**
Standard deviations		*0.05*	*1.48*	0.25	*0.001*	*60.59*
Standard error		*0.03*	*0.85*	*0.14*	*0.001*	*34.98*
Coefficient of variation		*2.33*	*2.30*	*2.33*	*0.26*	*2.26*
Error propagation (%)		*1.34*	*1.33*	*1.34*	*0.15*	*1.30*
HPFRC0-N15	0.375	1.63	48.96	11.75	0.30	4210.91
		1.82	54.52	13.08	0.34	4183.96
		1.72	51.73	12.41	0.38	3495.36
Average value		**1.72**	**51.74**	**12.42**	**0.34**	**3963.41**
Standard deviations		*0.09*	*2.78*	*0.67*	*0.04*	*405.56*
Standard error		*0.05*	*1.61*	*0.39*	*0.02*	*234.15*
Coefficient of variation (%)		*5.23*	*5.37*	*5.39*	*11.76*	*10.23*
Error propagation (%)		*3.02*	*3.10*	*3.11*	*6.79*	*5.91*
HPFRC1 series						
HPFRC1-N00	0.00	12.47	373.95	35.06	1.21	2278.94
		13.44	403.21	37.80	1.25	2374.44
		11.88	356.28	33.40	1.20	2196.63
Average value		**12.59**	**377.82**	***35.42***	**1.22**	**2283.34**
Standard deviations		*0.79*	*23.70*	*2.22*	*0.03*	*88.99*
Standard error		*0.46*	*13.68*	*1.28*	*0.02*	*51.38*
Coefficient of variation (%)		*6.27*	*6.27*	*6.27*	*2.46*	*3.90*
Error propagation (%)		*3.62*	*3.62*	*3.62*	*1.42*	*2.25*
HPFRC1-N05	0.125	10.48	314.32	38.49	1.20	2736.78
		9.84	295.27	36.16	1.19	2573.37
		10.23	306.99	37.59	1.17	2741.45
Average value		**10.18**	**305.53**	**37.41**	**1.19**	**2683.87**
Standard deviations		*0.32*	*9.61*	*1.18*	*0.02*	*95.72*

TABLE 4 (Continued)

Test series		Force, P_{MOR}	Moment, M_{MOR}	Flexural strength, f_{MOR}	Deflection, δ_{MOR}	Elastic modulus, E
—	Ratio of $\alpha = \frac{a}{h}$	(kN)	(kN mm)	(MPa)	(mm)	(MPa)
Standard error		*0.18*	*5.55*	*0.68*	*0.01*	*55.26*
Coefficient of variation (%)		*3.14*	*3.15*	*3.15*	*1.68*	*3.57*
Error propagation (%)		*1.81*	*1.82*	*1.82*	*0.97*	*2.06*
HPFRC1-N10	0.250	6.92	207.59	34.60	1.04	3143.97
		7.93	237.82	39.64	0.98	3792.21
		7.13	214.01	35.67	0.91	3702.48
Average value		**7.33**	**219.81**	**36.63**	**0.98**	**3546.22**
Standard deviations		*0.53*	*15.92*	*2.65*	*0.06*	*351.24*
Standard error		*0.31*	*9.19*	*1.53*	*0.03*	*202.79*
Coefficient of variation (%)		*7.23*	*7.24*	*7.23*	*6.12*	*9.90*
Error propagation (%)		*4.17*	*4.18*	*4.18*	*3.53*	*5.72*
HPFRC1-N15	0.375	4.32	129.61	31.11	0.84	3978.66
		4.47	134.08	32.18	0.85	4058.26
		4.32	129.57	31.10	0.86	3914.02
Average value		**4.37**	**131.08**	**31.46**	**0.85**	**3983.65**
Standard deviations		*0.09*	2.59	*0.62*	*0.01*	*72.25*
Standard error		*0.05*	*1.50*	*0.36*	*0.01*	*41.71*
Coefficient of variation (%)		*2.06*	*1.98*	*1.97*	*1.18*	*1.81*
Error propagation (%)		*1.19*	*1.14*	*1.14*	*0.68*	*1.05*
HPFRC2 series						
HPFRC2-N00	0.00	11.07	332.19	31.14	1.18	2076.77
		11.14	334.28	31.34	1.16	2128.50
		10.54	316.35	29.66	1.09	2133.74
Average value		**10.92**	**327.61**	**30.71**	**1.15**	**2113.00**
Standard deviations		*0.33*	*9.81*	*0.92*	*0.04*	*31.49*
Standard error		*0.19*	*5.66*	*0.53*	*0.02*	*18.18*
Coefficient of variation (%)		*3.02*	*2.99*	*3.00*	*3.48*	*1.49*
Error propagation (%)		*1.74*	*1.73*	*1.73*	*2.01*	*0.86*
HPFRC2-N05	0.125	8.56	256.87	31.45	1.02	2628.04
		8.62	258.52	31.66	1.04	2575.94
		8.82	264.64	32.40	1.14	2418.42
Average value		**8.67**	**260.01**	**31.84**	**1.07**	**2540.80**
Standard deviations		*0.14*	*4.09*	*0.50*	*0.06*	*109.14*
Standard error		*0.08*	*2.36*	*0.29*	*0.03*	*63.01*
Coefficient of variation (%)		*1.61*	*1.57*	*1.57*	*5.61*	*4.30*
Error propagation (%)		*0.93*	*0.91*	*0.91*	*3.24*	*2.48*
HPFRC2-N10	0.250	5.31	159.16	26.53	1.00	2486.09
		6.77	203.18	33.86	0.92	3473.70
		6.66	199.90	33.32	0.92	3417.86
Average value		**6.25**	**187.41**	**31.24**	**0.95**	**3125.88**
Standard deviations		*0.82*	*24.52*	*4.09*	*0.05*	*554.78*
Standard error		*0.47*	*14.16*	*2.36*	*0.03*	*320.30*
Coefficient of variation (%)		*13.12*	*13.08*	*13.09*	*5.26*	*17.75*
Error propagation (%)		*7.57*	*7.55*	*7.56*	*3.04*	*10.25*
HPFRC2-N15	0.375	4.32	129.66	31.12	0.82	4107.34
		4.40	132.04	31.69	0.82	4150.89
		3.87	116.05	27.85	0.80	3755.57

(Continues)

TABLE 4 (Continued)

Test series		Force, P_{MOR}	Moment, M_{MOR}	Flexural strength, f_{MOR}	Deflection, δ_{MOR}	Elastic modulus, E
—	Ratio of $\alpha = \frac{a}{h}$	(kN)	(kN mm)	(MPa)	(mm)	(MPa)
Average value		**4.20**	**125.92**	**30.22**	**0.81**	**4004.60**
Standard deviations		*0.29*	*8.63*	*2.07*	*0.01*	*216.76*
Standard error		*0.17*	*4.98*	*1.20*	*0.01*	*125.15*
Coefficient of variation (%)		*6.90*	*0.07*	*0.07*	*0.01*	*0.05*
Error propagation (%)		*3.99*	*3.96*	*3.95*	*0.71*	*3.13*

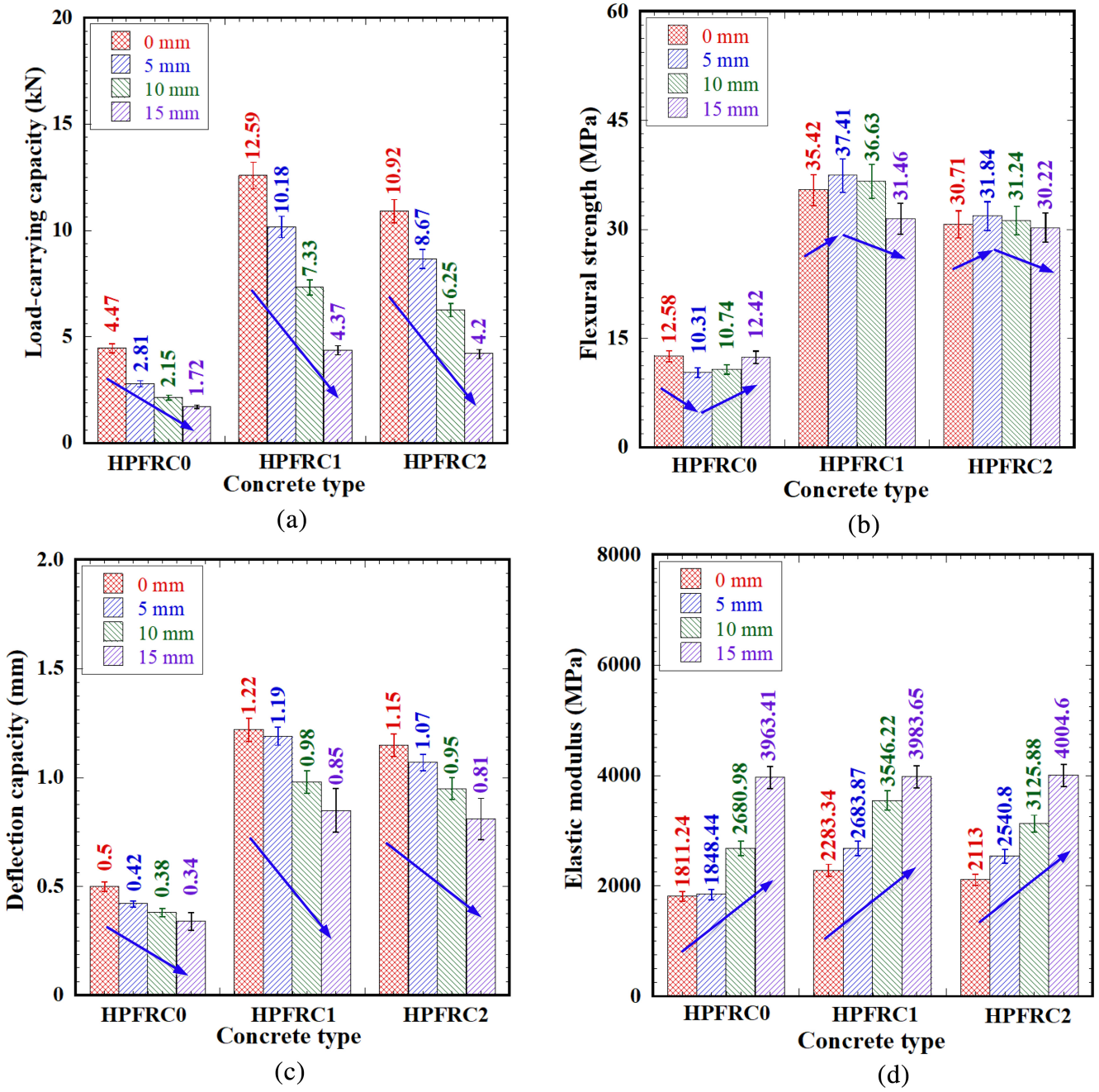


FIGURE 10 Comparison of flexural strength and deflection capacity of the studied concretes. (a) Load-carrying capacity. (b) Flexural strength. (c) Deflection capacity. (d) Elastic modulus.

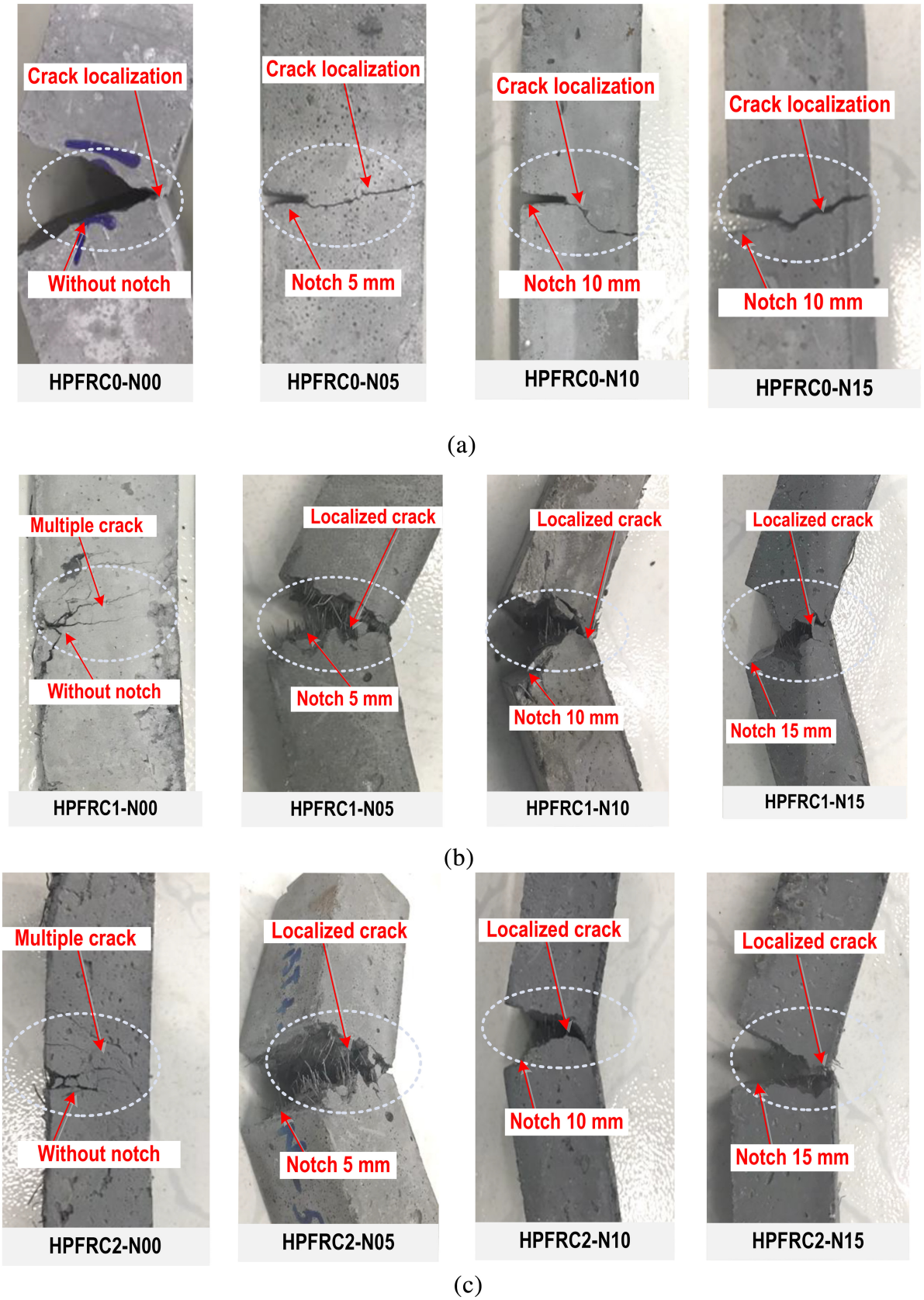


FIGURE 11 Regression of mechanical properties of HPFRCs with notch-to-depth ratio. (a) HPFRC0 series; (b) HPFRC1 series; (c) HPFRC2 series.

capacity ($\Delta P_{max} = P_{max} - P_{min} = 40\%P_{MOR} \div 90\%P_{MOR}$). During the fatigue test, the maximum load at each cycle and the number of cycles to failure were recorded. This study evaluated the S-N Wöhler curve of HPFRC, with the vertical axis represented by $S = \Delta f_{max}/f_{MOR}$ and $S = \Delta f_{max}/f_{MOR}$. A minimum cyclic load of $P_{min} = 1$kN was applied to ensure positive bending during testing, while maximum cyclic load (P_{max}) must be less than P_{MOR}, that is, $0 < f_{min} < f_{max} < f_{MOR}$. Figure 6 shows the cyclic load with a period of $T = 0.05$s used in flexural fatigue test. The following section presents the results and discussion, including detailed comparisons of the flexural behavior of HPFRC specimens with different notch depths and loading conditions.

4 | RESULTS AND DISCUSSION

4.1 | Static behavior of the HPFRC specimens with different notch depths

The flexural response curves of HPFRC specimens with different fiber systems were plotted for HPFRC0 (Figure 7), HPFRC1 (Figure 8), and HPFRC2 (Figure 9). In these figures, the left vertical axis represents flexural strength, while the right vertical axis indicates the applied load. The responses of four different initial notch depths are presented as follows: N00 in Figures 7a, 8a, and 9a, N05 in Figures 7b, 8b, and 9b, N10 in Figures 7c, 8c, and 9c, and N15 in Figures 7d, 8d, and 9d. Table 4

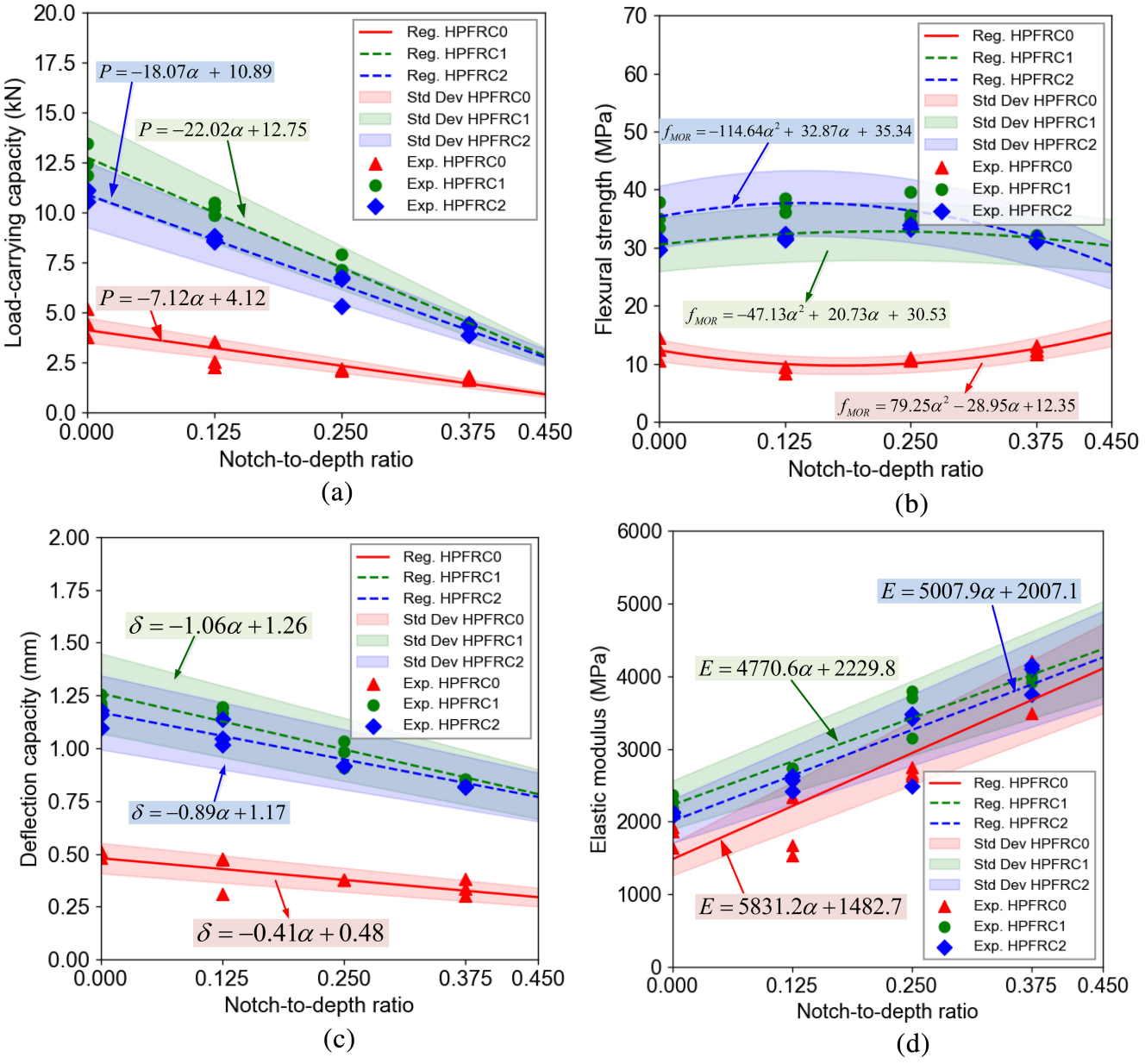


FIGURE 12 Photos of flexural failure specimens of the studied HPFRCs under static loading. (a) Load-carrying capacity according to N/D. (b) Flexural strength according to N/D. (c) Deflection capacity according to N/D. (d) Elastic modulus according to N/D.

TABLE 5 Fracture parameters of the notched HPFRC specimen.

Test series	Ratio of $\alpha = \frac{a}{h}$	Elastic modulus, E (MPa)	Maximum moment, M_{MOR} (kN mm)	Critical stress intensity factor, K_{IC} (MPa)	Critical strain energy release rate, G_{IC} (kJ/m^2)
HPFRC0 series [26]					
HPFRC0-N05 (Notch 5 mm)	0.125	1529.47	69.06	0.83	0.45
		2339.34	106.43	1.28	0.70
		1676.51	77.14	0.92	0.51
Average value		**1848.44**	**84.21**	**1.01**	**0.55**
Standard deviations		*431.44*	*19.66*	*0.24*	*0.13*
Standard error		*249.09*	*11.35*	*0.14*	*0.08*
Coefficient of variation (%)		*0.23*	*0.23*	*0.24*	*0.24*
Error propagation (%)		*13.48*	*13.48*	*13.72*	*13.65*
HPFRC0-N10 (Notch 10 mm)	0.250	2629.98	63.15	0.73	0.20
		2664.99	64.16	0.74	0.20
		2747.96	66.07	0.76	0.21
Average value		**2680.98**	**64.46**	**0.74**	**0.20**
Standard deviations		*60.59*	*1.48*	*0.02*	*0.005*
Standard error		*34.98*	*0.85*	*0.01*	*0.00*
Coefficient of variation (%)		*0.02*	*0.02*	*0.03*	*0.03*
Error propagation (%)		*1.30*	*1.33*	*1.56*	*1.44*
HPFRC0-N15 (Notch 15 mm)	0.375	4210.91	48.96	0.55	0.07
		4183.96	54.52	0.62	0.09
		3495.36	51.73	0.58	0.10
Average value		**3963.41**	**64.46**	**0.58**	**0.09**
Standard deviations		*405.56*	*1.48*	*0.03*	*0.01*
Standard error		*234.15*	*0.85*	*0.02*	*0.01*
Coefficient of variation (%)		*0.10*	*0.02*	*0.05*	*0.11*
Error propagation (%)		*5.91*	*1.33*	*2.99*	*6.42*
HPFRC1 series					
HPFRC1-N05 (Notch 5 mm)	0.125	2736.78	373.95	4.48	7.34
		2573.37	403.21	4.83	9.08
		2741.45	356.28	4.27	6.65
Average value		**2683.87**	***377.82***	***4.53***	**7.69**
Standard deviations		*95.72*	*23.7*	*0.28*	*1.25*
Standard error		*55.26*	*13.68*	*0.16*	*0.72*
Coefficient of variation (%)		*0.04*	*0.06*	*0.06*	*0.16*
Error propagation (%)		*2.06*	*3.62*	*3.57*	*9.38*
HPFRC1-N10 (Notch 10 mm)	0.250	3143.97	314.32	3.61	4.15
		3792.21	295.27	3.39	3.03
		3702.48	306.99	3.53	3.36
Average value		**3546.22**	**305.53**	**3.51**	**3.51**
Standard deviations		*351.24*	*9.61*	*0.11*	*0.57*
Standard error		*202.79*	*5.55*	*0.06*	*0.33*
Coefficient of variation (%)		*0.10*	*0.03*	*0.03*	*0.16*
Error propagation (%)		*5.72*	*1.82*	*1.81*	*9.38*

(Continues)

TABLE 5 (Continued)

Test series	Ratio of $\alpha = \frac{a}{h}$	Elastic modulus, E (MPa)	Maximum moment, M_{MOR} (kN mm)	Critical stress intensity factor, K_{IC} (MPa)	Critical strain energy release rate, G_{IC} (kJ/m^2)
HPFRC1-N15 (Notch 15 mm)	0.375	3978.66	207.59	2.49	1.56
		4058.26	237.82	2.85	2.00
		3914.02	214.01	2.57	1.68
Average value		**3983.65**	**219.81**	**2.63**	**1.75**
Standard deviations		*72.25*	*15.92*	*0.19*	*0.23*
Standard error		*41.71*	*9.19*	*0.11*	*0.13*
Coefficient of variation (%)		*0.02*	*0.07*	*0.07*	*0.13*
Error propagation (%)		*1.05*	*4.18*	*4.17*	*7.59*
HPFRC2 series					
HPFRC2-N05 (Notch 5 mm)	0.125	2628.04	332.19	3.98	6.03
		2575.94	334.28	4.01	6.23
		2418.42	316.35	3.79	5.95
Average value		**2540.80**	**327.61**	**3.93**	**6.07**
Standard deviations		*109.14*	*9.81*	*0.12*	*0.15*
Standard error		*63.01*	*5.66*	*0.07*	*0.09*
Coefficient of variation (%)		*0.04*	*0.03*	*0.03*	*0.02*
Error propagation (%)		*2.48*	*1.73*	*1.76*	*1.43*
HPFRC2-N10 (Notch 10 mm)	0.250	2486.09	256.87	2.95	3.50
		3473.70	258.52	2.97	2.54
		3417.86	264.64	3.04	2.70
Average value		**3125.88**	**260.01**	**2.99**	**2.91**
Standard deviations		*554.78*	*4.09*	*0.05*	*0.52*
Standard error		*320.30*	*2.36*	*0.03*	*0.30*
Coefficient of variation (%)		*0.18*	*0.02*	*0.02*	*0.18*
Error propagation (%)		*10.25*	*0.91*	*0.97*	*10.32*
HPFRC2-N15 (Notch 15 mm)	0.375	4107.34	159.16	1.91	0.89
		4150.89	203.18	2.44	1.43
		3755.57	199.90	2.40	1.53
Average value		**4004.60**	**187.41**	**2.25**	**1.28**
Standard deviations		*216.76*	*24.52*	*0.29*	*0.35*
Standard error		*125.15*	*14.16*	*0.17*	*0.20*
Coefficient of variation (%)		*0.05*	*0.13*	*0.13*	*0.27*
Error propagation (%)		*3.13*	*7.55*	*7.44*	*15.79*

shows the experimental results of the HPFRC0, HPFRC1, and HPFRC2 subject to flexural static loading, including peak force (P_{MOR}), peak moment (M_{MOR}), flexural strength at MOR (f_{MOR}), deflection at MOR (δ_{MOR}), and elastic modulus (E). The P_{MOR} changed from 1.72 to 12.59 kN, the f_{MOR} ranged from 10.31 to 37.41 MPa, the δ_{MOR} varied from 0.34 to 1.22 mm, the E was observed from 1811.24 to 4004.60 MPa. As can be seen from Figures 7–9, the static behaviors of HPFRCs were significantly improved with the presence of embedded hybrid fibers. The HPFRC0 with no fiber exhibited unstable failure characterized by a sudden load drop, while both HPFRC1 and HPFRC2 revealed stable failure with a gentle load reduction after their peaks. Among the three, HPFRC1 produced the highest values of P_{MOR} (12.59 kN), f_{MOR} (37.41 MPa), δ_{MOR} (1.22 mm), as shown in

Figure 10. Except in the case of no-notch specimen, as the notch depth of the specimen increased, the f_{MOR} of HPFRC0 increased, while the f_{MOR} of HPFRC1 and HPFRC2 decreased. The f_{MOR} trend observed in HPFRC0 can be explained by the size effect law for brittle or quasi-brittle materials,[27] that is, a smaller specimen section results in a higher strength. Figure 11 shows the photos of failure specimens of the HPFRCs under static loading. For notched specimen, a single critical crack was always initiated from the notch end (crack tip) and extended toward the specimen top. The HPFRC0 with no fiber showed entirely separated fractures, whereas the HPFRC1 and HPFRC2 with embedded fibers did not fully separate. The fibers at the failure cracks were pulled out

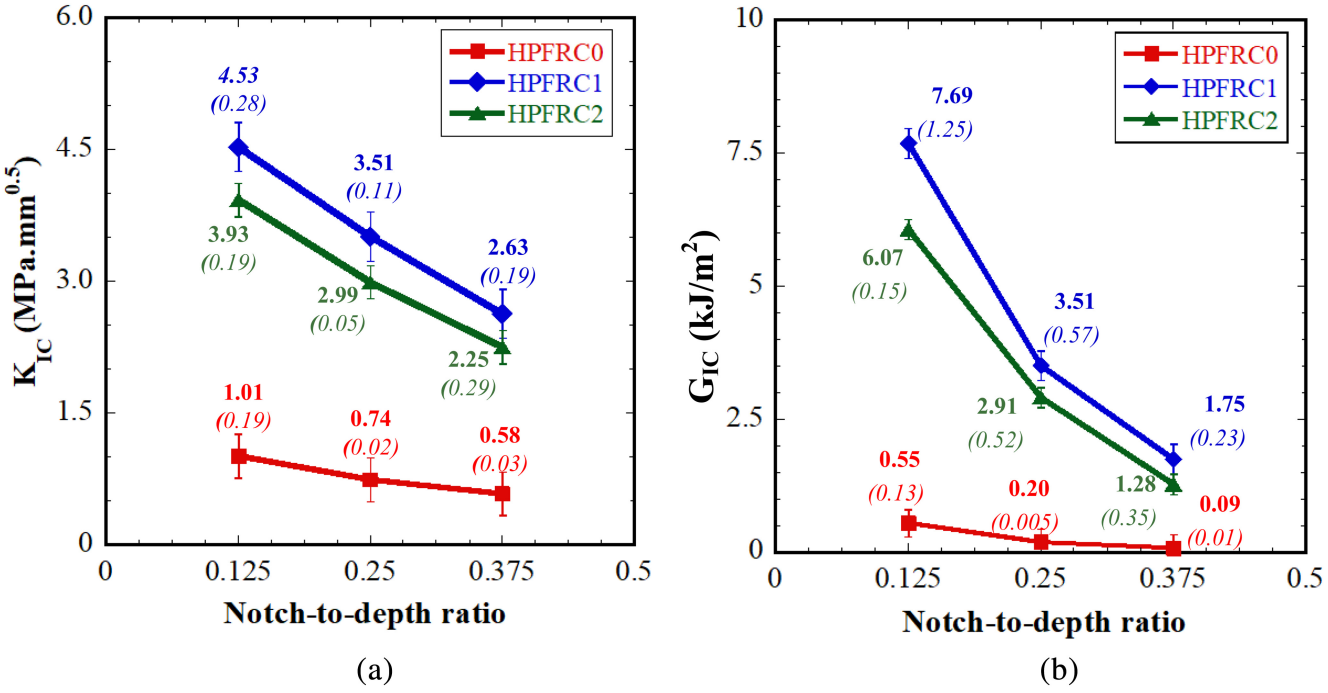


FIGURE 13 K_{IC} and G_{IC} of HPFRCs with various depth notch. (a) Critical stress intensity factor; (b) Critical strain energy release rate.

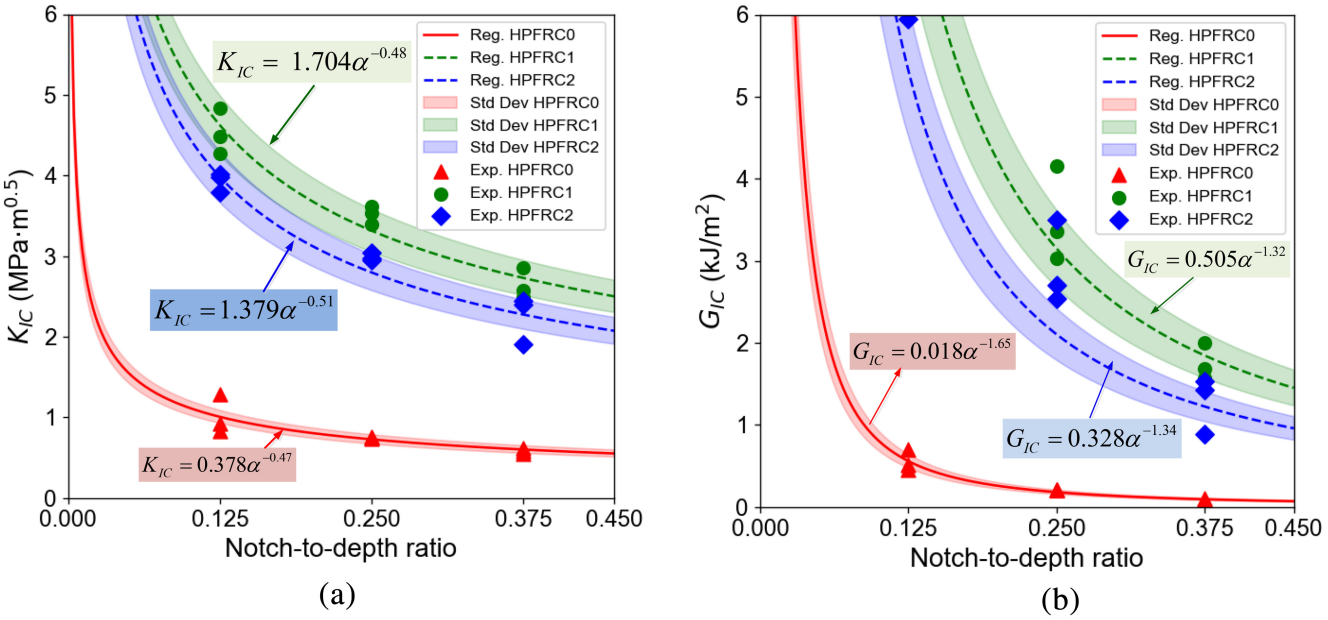


FIGURE 14 Regression of K_{IC} and G_{IC} of HPFRCs with various notch-to-depth ratio. (a) K_{IC}; (b) G_{IC}.

rather than broken, indicating debonding between the steel fibers and the concrete matrix.[46]

4.2 | Modeling flexural parameters regarding notch-to-depth ratio under static load

To forecast the parameters of P_{MOR}, δ_{MOR}, and E under static load with respect to N/D ratio (α), a linear function following the parameter trends, shown in Figure 10, was chosen to fit the experimental data as given in Equation (4). Besides, a parabolic function, $f_{MOR}(\alpha)$, following the f_{MOR} trend was employed to mathematically model using Equation (5).

$$y(\alpha) = p + q\alpha, \alpha \neq 0, \tag{4}$$

$$f_{MOR}(\alpha) = a\alpha^2 + b\alpha + c, a \neq 0. \tag{5}$$

For determining the coefficients of Equations (4) and (5), regression analyses were performed with different specimen depth-notch for the HPFRC0, HPFRC1, and HPFRC2. The regression functions of the P_{MOR}, δ_{MOR}, and E were presented in Figure 12a,c,d, respectively, that of the f_{MOR} was shown in Figure 12b. The regression models in Figure 12 highlight the influence of the notch-to-depth ratio on the mechanical properties of HPFRCs. The coefficients of Equations (4) and (5) also reflect physical behavior. Negative slopes in load and deflection capacity indicate reduced performance with increased notching, whereas higher values reflect greater notch sensitivity (Figure 12a,b). The quadratic terms in flexural strength capture nonlinear trends, suggesting an optimal notch level at 5 mm (Figure 12c). Although the elastic modulus shows an increasing trend, this may be attributed to fiber-induced stiffness effects and stress redistribution (Figure 12d).

4.3 | Fracture parameters of notched HPFRC specimens under bending

4.3.1 | The critical stress intensity factor and critical energy release rate

Fracture parameters indicate material properties to resist crack initiation and propagation under loading. In this study, the crack propagation regarding mode I was investigated based on the fracture toughness. In Mode I, the critical stress intensity factor (K_{IC}) of the HPFRCs under 3 PB loading can be obtained using Equation (6).[47] The energy release rate (G_{IC}), defined as energy released per unit crack extension area,[48] was also derived using Equation (7).

$$K_{IC} = 6Y(\alpha)M_{MOR} \times \frac{\sqrt{a}}{bh^2}, \tag{6}$$

$$G_{IC} = \frac{K^2_{IC}}{E} = \frac{36 \times Y^2(\alpha) \times M^2_{MOR} \times a}{b^2 \times h^4 \times E}, \tag{7}$$

$$Y(\alpha) = \frac{[1.99 - \alpha \times (1-\alpha)(2.15 - 3.93\alpha + 2.7\alpha^2)]}{(1+2\alpha)(1-\alpha)^{3/2}}; \quad 0 < \alpha = \frac{a}{h} < 1, \tag{8}$$

where M_{MOR} is the moment at modulus of rupture; E is the elastic modulus; a, b, and h denote the notched depth, section width, and section depth of bending specimen, respectively. It is noticeable that the $Y(\alpha)$ given in Equation (8) will vary consistently in the α range of [0.125, 0.165] and will vary inversely in the α range of [0.165, 0.375]. Table 5 and Figure 13 show the K_{IC} and G_{IC} of the HPFRCs with the $\alpha = 0.125$, 0.250, and 0.375. Obviously, the presence of the reinforcing fibers produced an improvement in fracture resistance. The K_{IC} value was in the range of 0.77–4.53 MPa. $\sqrt{m}$ and the G_{IC} changed from 0.14 to 3.88 MPa mm. As can show in Figure 13, the K_{IC} and G_{IC} of the HPFRCs decreased with the increase in α.

4.3.2 | Modeling critical stress intensity factor and the energy release rate

To predict the K_{IC} and G_{IC} of HPFRCs according to α value, an exponential function following the parameter

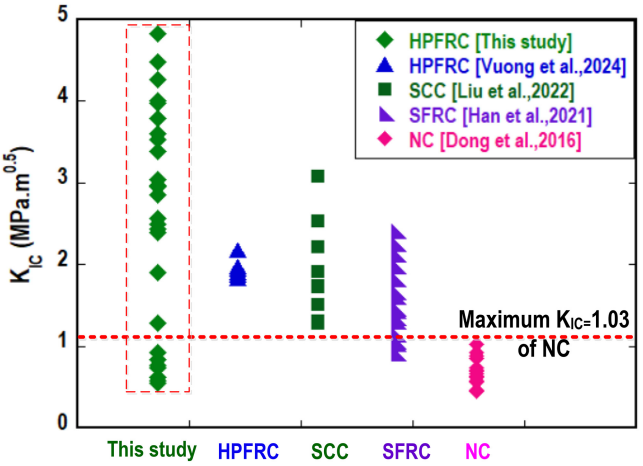


FIGURE 15 Comparison of K_{IC} regarding various concrete.

trends, as shown in Figure 13, was chosen to fit the experimental data using Equation (9). Using regression analysis to find the coefficients m and n, the model equations of the K_{IC} and G_{IC} were given by Equations (10) and (11), respectively, then displayed in Figure 14.

$$g(\alpha) = m \times \alpha^n, \tag{9}$$

$$\begin{cases} \text{for HPFRC0}: K_{IC} = 0.378\alpha^{-0.47} & \text{with } R^2 = .67 \\ \text{for HPFRC1}: K_{IC} = 1.704\alpha^{-0.48} & \text{with } R^2 = .93, \\ \text{for HPFRC2}: K_{IC} = 1.379\alpha^{-0.51} & \text{with } R^2 = .93 \end{cases} \tag{10}$$

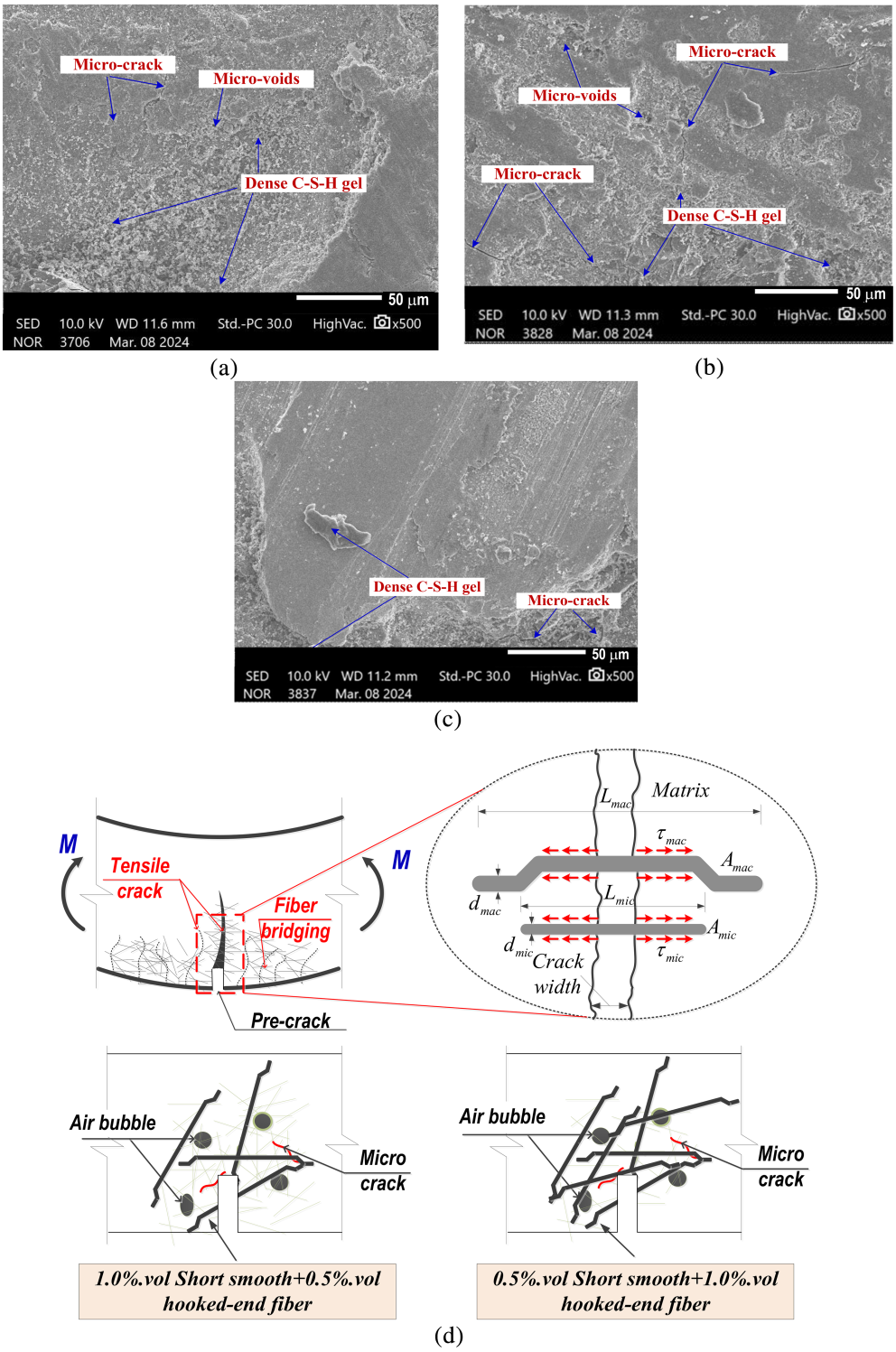


FIGURE 16 SEM analysis and fiber bridging mechanism in HPFRCs. (a) SEM of HPFRC0; (b) SEM of HPFRC1; (c) SEM of HPFRC; (d) Fiber bridging mechanism in HPFRC mixture.

$$\begin{cases} \text{for HPFRC0}: G_{IC} = 0.018\alpha^{-1.65} & \text{with } R^2 = .91 \\ \text{for HPFRC1}: G_{IC} = 0.505\alpha^{-1.32} & \text{with } R^2 = .93 \\ \text{for HPFRC2}: G_{IC} = 0.328\alpha^{-1.34} & \text{with } R^2 = .95 \end{cases} . \quad (11)$$

As can be seen Figure 14, both the parameters of K_{IC} and G_{IC} exhibit decreasing trends with increasing notch-to-depth ratio, their coefficients also reflect key physical performance. The negative exponents in the power-law models indicate a strong inverse relationship, where both K_{IC} and G_{IC} as the notch severity increases. For example, the HPFRC1 (1.0% long hooked blending 0.5% short smooth fiber) exhibits higher coefficient values and less negative exponents, suggesting improved resistance to crack initiation and propagation, and reduced sensitivity to notching effects. Figure 15 shows the K_{IC} of various cementitious composite types as reported in previous studies[49–52]: the studied concrete shows a similar value to other HPFRCs,[49] 1.56 times higher than that of self-compacting concrete (SCC),[50] 2.00 times higher than steel fiber-reinforced concrete (SFRC),[51] and 4.69 times higher than normal concrete (NC).[52] Figure 16a–c show SEM micrographs at 28 days of age for HPFRC0, HPFRC1, and HPFRC2, respectively. Each SEM was captured at 500× magnification with a resolution of 1280 × 1024 pixels. All three mixtures exhibit similarly dense microstructures, indicating a uniformly compact HPFRC matrix. Figure 16d displays the fiber pull-out and crack bridging mechanisms, highlighting features as air bubbles and tiny cracks inside the HPFRCs. A higher volume of embedded long hooked fibers increases the probability of them crossing the air bubbles and tiny cracks, resulting in a higher K_{IC}. In contrast, increasing the content of short smooth fibers did not improve crack-bridging efficiency, leading to a decrease in K_{IC}.[49] In HPFRC mixtures with hybrid fibers, long-hooked and short-smooth fibers contribute in markedly different ways. The characteristic strain-hardening behavior of hybrid fiber-reinforced concrete is primarily governed by the long-hooked fibers rather than the short-smooth fibers.[53] Consequently, long fibers was thought to play the dominant role in resisting crack initiation and propagation compared with short fibers.

4.3.3 | Crack mouth opening displacement

Figure 17 illustrates the crack mouth opening displacement (w_c) of a notched specimen at MOR under 3 PB. The w_c can be calculated according to notch-to-depth ratio (α), as presented in Equation (12)[54]:

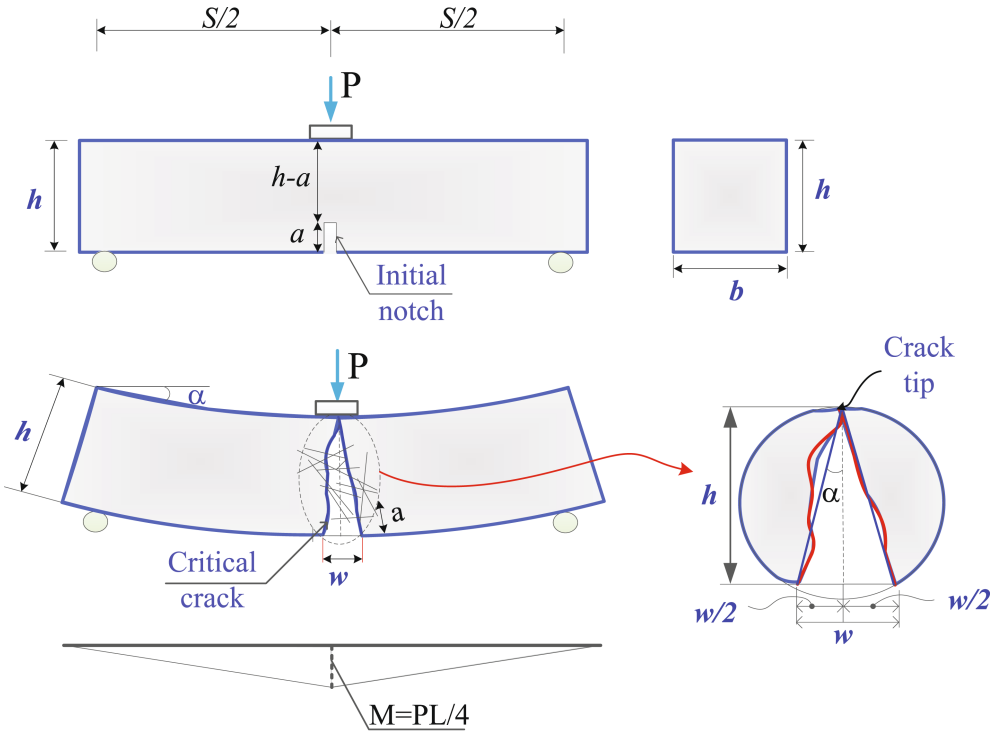


FIGURE 17 Schematic diagram of a notched specimen instrumented under 3PB test.

TABLE 6 Deflection capacity and crack mouth opening displacement of the notched HPFRC specimen.

Test series —	Ratio of $\alpha = \frac{a}{h}$	Elastic modulus, E (MPa)	Deflection, δ_{MOR} (mm)	Flexural strength, f_{MOR} (MPa)	Crack mouth opening displacement, w_c (mm)
HPFRC0 series					
HPFRC0-N05 (Notch 05 mm)	0.125	1529.47	0.47	8.46	0.15
		2339.34	0.47	13.03	0.15
		1676.51	0.48	9.45	0.15
Average value		**1848.44**	**0.47**	**10.31**	**0.15**
Standard deviations		*431.44*	*0.09*	*2.41*	0.001
Standard error (%)		*249.09*	*0.05*	*1.39*	*0.00*
Coefficient of variation		*23.34*	*19.15*	*23.38*	*0.67*
Error propagation (%)		*13.48*	*11.06*	*13.50*	*0.38*
HPFRC0-N10 (Notch 10 mm)	0.250	2629.98	0.38	10.53	0.25
		2664.99	0.38	10.69	0.25
		2747.96	0.38	11.01	0.25
Average value		**2680.98**	**0.38**	**10.74**	**0.25**
Standard deviations		*60.59*	*0.001*	0.25	*0.0003*
Standard error		*34.98*	*0.001*	*0.14*	*0.0002*
Coefficient of variation (%)		*0.02*	*0.003*	*0.02*	*0.0012*
Error propagation (%)		*1.30*	*0.15*	*1.34*	*0.069*
HPFRC0-N15 (Notch 15 mm)	0.375	4210.91	0.30	11.75	0.33
		4183.96	0.34	13.08	0.37
		3495.36	0.38	12.41	0.42
Average value		**3963.41**	**0.34**	**12.42**	**0.37**
Standard deviations		*405.56*	*0.04*	*0.67*	*0.05*
Standard error		*234.15*	*0.02*	*0.39*	*0.03*
Coefficient of variation (%)		*0.10*	*0.12*	*0.05*	*0.14*
Error propagation (%)		*5.91*	*6.79*	*3.11*	*7.80*
HPFRC1 series					
HPFRC1-N05 (Notch 05 mm)	0.125	2736.78	1.20	38.49	0.38
		2573.37	1.19	36.16	0.38
		2741.45	1.17	37.59	0.37
Average value		**2683.87**	**1.19**	**37.41**	**0.38**
Standard deviations		*95.72*	*0.02*	*1.18*	*0.01*
Standard error		*55.26*	*0.01*	*0.68*	*0.01*
Coefficient of variation (%)		*3.57*	*1.68*	*3.15*	*2.63*
Error propagation (%)		*2.06*	*0.97*	*1.82*	*1.52*
HPFRC1-N10 (Notch 10 mm)	0.250	3143.97	1.04	34.60	0.67
		3792.21	0.98	39.64	0.64
		3702.48	0.91	35.67	0.59
Average value		**3546.22**	**0.98**	**36.63**	**0.63**
Standard deviations		*351.24*	*0.06*	*2.65*	*0.04*
Standard error		*202.79*	*0.03*	*1.53*	*0.02*
Coefficient of variation (%)		*9.90*	*6.12*	*7.23*	*6.35*
Error propagation (%)		*5.72*	*3.53*	*4.18*	*3.67*

(Continues)

TABLE 6 (Continued)

Test series —	Ratio of $\alpha = \frac{a}{h}$	Elastic modulus, E (MPa)	Deflection, δ_{MOR} (mm)	Flexural strength, f_{MOR} (MPa)	Crack mouth opening displacement, w_c (mm)
HPFRC1-N15 (Notch 15 mm)	0.375	3978.66	0.84	31.11	0.93
		4058.26	0.85	32.18	0.94
		3914.02	0.86	31.10	0.94
Average value		**3983.65**	**0.85**	**31.46**	**0.94**
Standard deviations		*72.25*	*0.01*	*0.62*	*0.01*
Standard error		*41.71*	*0.01*	*0.36*	*0.01*
Coefficient of variation (%)		*1.81*	*1.18*	*1.97*	*1.06*
Error propagation (%)		*1.05*	*0.68*	*1.14*	*0.61*
HPFRC2 series					
HPFRC2-N05 (Notch 05 mm)	0.125	2628.04	1.02	31.45	0.33
		2575.94	1.04	31.66	0.33
		2418.42	1.14	32.40	0.37
Average value		**2540.80**	**1.07**	**31.84**	**0.34**
Standard deviations		*109.14*	*0.06*	*0.50*	*0.02*
Standard error		*63.01*	*0.03*	*0.29*	*0.01*
Coefficient of variation (%)		*4.30*	*5.61*	*1.57*	*5.88*
Error propagation (%)		*2.48*	*3.24*	*0.91*	*3.40*
HPFRC2-N10 (Notch 10 mm)	0.250	2486.09	1.00	26.53	0.65
		3473.70	0.92	33.86	0.53
		3417.86	0.92	33.32	0.53
Average value		**3125.88**	**0.95**	**31.24**	**0.57**
Standard deviations		*554.78*	*0.05*	*4.09*	*0.07*
Standard error		*320.30*	*0.03*	*2.36*	*0.04*
Coefficient of variation (%)		*17.75*	*5.26*	*13.09*	*12.28*
Error propagation (%)		*10.25*	*3.04*	*7.56*	*7.09*
HPFRC2-N15 (Notch 15 mm)	0.375	4107.34	0.82	31.12	0.90
		4150.89	0.82	31.69	0.91
		3755.57	0.80	27.85	0.88
Average value		**4004.60**	**0.81**	**30.22**	**0.90**
Standard deviations		*216.76*	*0.01*	*2.07*	*0.01*
Standard error		*125.15*	*0.01*	*1.20*	*0.01*
Coefficient of variation (%)		*5.41*	*1.23*	*6.85*	*1.11*
Error propagation (%)		*3.13*	*0.71*	*3.95*	*0.64*

$$w_c = \frac{4 f_{MOR}}{E} \upsilon_\beta(\alpha), \tag{12}$$

$$\upsilon_\beta(\alpha) = 0.8 - 1.7\alpha + 2.4\alpha^2 + \frac{0.66}{(1-\alpha)^2} + \frac{4}{\beta}\Big(-0.04 - 0.58\alpha + 1.47\alpha^2 - 2.04\alpha^3 \Big), \tag{13}$$

where $\beta = 3$ is the ratio of span to depth of flexural specimen.

Table 6 provides the fracture parameters of the notched specimens with different α values, while Figure 18 displays the w_c of the HPFRCs according to different notch depths, ranging from 0.15 to 0.94 mm. As displayed in Figure 18, the w_c increased clearly with the increase in α from 0.125 to 0.375; this trend is wholly consistent with that in previous investigation conducted by Yin et al.[21] As the α increased, the w_c and f_{MOR} had the same trend for HPFRC0, but opposite trend for HPFRC1 and HPFRC2. It is noticeable that the $\upsilon_\beta(\alpha)$, as

expressed by Equation (13), will increase as the α increases in range of [0.1, 0.5].

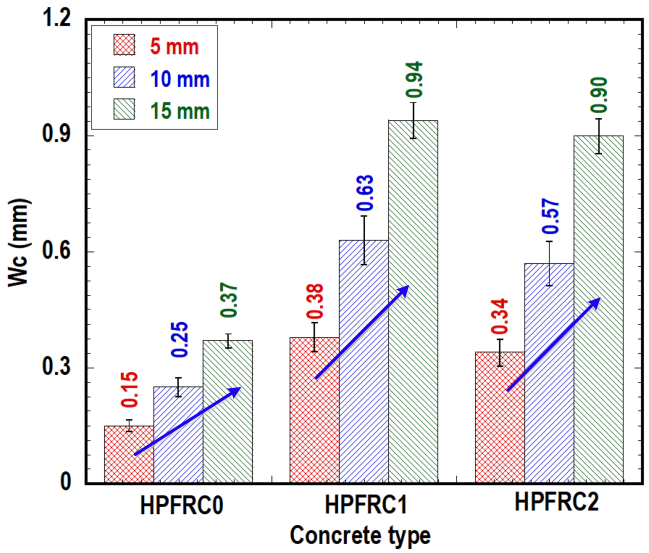


FIGURE 18 Fracture parameter of HPFRC series with various notch-to-depth ratio.

According to fracture mechanics, fracture process zone (FPZ) at the tip of the pre-cut notch plays the main role in crack developing,[19] which strongly correlates with the w_c of the flexural HPFRC specimen. Figure 19 shows the stress distributions and cohesive crack model with an initial crack. As shown in this figure, the bridging effect of fibers at crack helps in resisting to crack mouth opening. Besides, the higher notch depth (i.e., higher α), the lower uncracked zone of the failure section, this leads to a reduction in specimen stiffness and consequently an increment in the w_c.

4.4 | Fatigue behavior of HPFRC specimen with different notch-to-depth ratios

4.4.1 | Endurance limit of HPFRCs

Table 7 summarizes the results of HPFRC specimens with different α under cyclic loading. The maximum amplitude of load (ΔP_{max}), maximum amplitude of stress

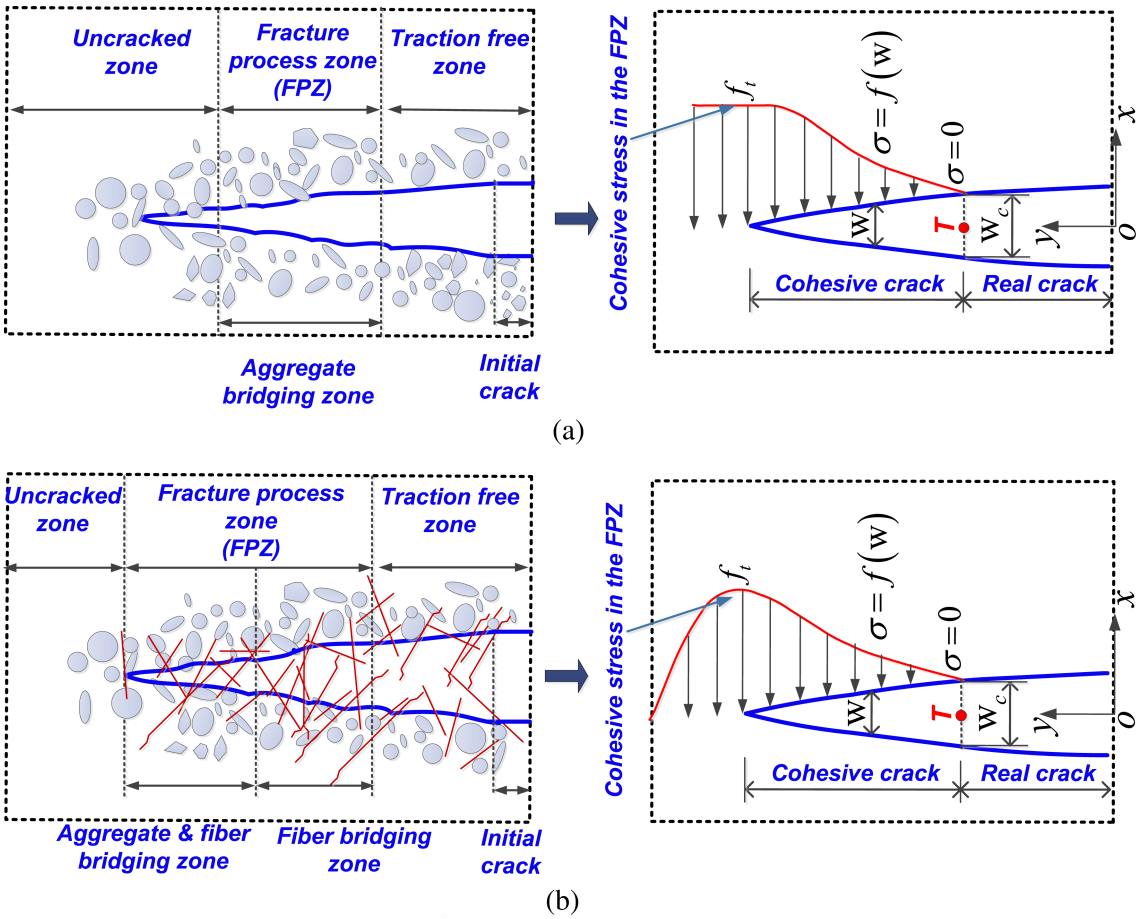


FIGURE 19 Stress distributions and cohesive crack model. (a) without fiber (brittle material); (b) With hybrid fiber (quasibrittle materials).

TABLE 7 Laboratory fatigue test results of the under cyclic loading.

HPFRC series	Test series	Maximum amplitude of load ΔP_{max} (kN)	Maximum amplitude of stress Δf_{max} (kPa)	Ratio $\frac{\Delta f_{max}}{f_{MOR}}$	Number of cycles N
HPFRC0 series	HPFRC0-N00 [39] (Notch 00 mm)	4.02	40.65	0.90	6
		3.13	31.62	0.70	15
		2.68	27.10	0.60	21
		2.24	22.59	0.50	26
		1.85	18.52	0.41	28
		1.34	13.55	0.30	320
		1.11	11.29	0.25	1657
		0.67	6.78	0.15	3689
		0.56	5.87	0.13	5266
		0.47	4.97	0.11	8273
	HPFRC0-N05 (Notch 05 mm)	4.02	40.65	0.90	4
		3.13	31.62	0.70	8
		2.68	27.10	0.60	12
		2.24	22.59	0.50	13
		1.79	18.07	0.40	21
	HPFRC0-N10 (Notch 10 mm)	4.02	40.65	0.90	3
		3.13	31.62	0.70	4
		2.68	27.10	0.60	10
		2.24	22.59	0.50	11
		1.79	18.07	0.40	18
	HPFRC0-N15 (Notch 15 mm)	4.02	40.65	0.90	2
		3.13	31.62	0.70	3
		2.68	27.10	0.60	7
		2.24	22.59	0.50	9
		1.79	18.07	0.40	15
HPFRC1 series	HPFRC1-N00 (Notch 00 mm)	11.33	114.54	0.90	186
		8.82	89.08	0.70	410
		7.56	76.36	0.60	17,102
		6.30	63.63	0.50	229,234
		5.04	50.91	0.40	610,212* (Not failure)
	HPFRC1-N05 (Notch 05 mm)	11.33	114.54	0.90	35
		8.82	89.08	0.70	88
		7.56	76.36	0.60	346
		6.30	63.63	0.50	99,360
		5.04	50.91	0.40	507,529* (Not failure)
	HPFRC1-N10 (Notch 10 mm)	11.33	114.54	0.90	9
		8.82	89.08	0.70	81
		7.56	76.36	0.60	248
		6.30	63.63	0.50	44,577
		5.04	50.91	0.40	

TABLE 7 (Continued)

HPFRC series	Test series	Maximum amplitude of load ΔP_{max} (kN)	Maximum amplitude of stress Δf_{max} (kPa)	Ratio $\frac{\Delta f_{max}}{f_{MOR}}$	Number of cycles N
					502,244* (Not failure)
	HPFRC1-N15 (Notch 15 mm)	11.33	114.54	0.90	4
		8.82	89.08	0.70	17
		7.56	76.36	0.60	102
		6.30	63.63	0.50	32,705
		5.04	50.91	0.40	80,546
HPFRC2 series	HPFRC2-N00 (Notch 00 mm)	9.83	99.31	0.90	232
		7.64	77.24	0.70	583
		6.55	66.21	0.60	17,102
		5.46	55.17	0.50	230,655
		4.37	44.14	0.40	604,199* (Not failure)
	HPFRC2-N05 (Notch 05 mm)	9.83	99.31	0.90	13
		7.64	77.24	0.70	123
		6.55	66.21	0.60	15,472
		5.46	55.17	0.50	173,650
		4.37	44.14	0.40	519,784* (Not failure)
	HPFRC2-N10 (Notch 10 mm)	9.83	99.31	0.90	7
		7.64	77.24	0.70	24
		6.55	66.21	0.60	582
		5.46	55.17	0.50	81,006
		4.37	44.14	0.40	508,088* (not failure)
	HPFRC2-N15 (Notch 15 mm)	9.83	99.31	0.90	5
		7.64	77.24	0.70	15
		6.55	66.21	0.60	82
		5.46	55.17	0.50	55,961
		4.37	44.14	0.40	60,317

*Indicates specimen that had not failed yet.

(Δf_{max}), fatigue stress ratio ($\Delta f_{max}/f_{MOR}$), number of cycles (N) were provided in Table 7. Figures 20–22 present the responses of load amplitude versus cycle number for HPFRC0, HPFRC1, and HPFRC2, respectively. As can be seen in these figures and Table 7, the increase of ΔP_{max} (also increase of $\Delta f_{max}/f_{MOR}$) always accompanied with the decrease of N, regardless HPFRC series. The higher notch depth generally caused the lower N. In addition, the N of HPFRC0 is greatly lower than that of HPFRC with reinforcing fibers, at same $\Delta f_{max}/f_{MOR}$ and same notch depth. Obviously, the steel fibers' presence contributed significantly to the engineering duty in limiting the crack growth thus extending the fatigue life of the HPFRCs.

The reduction in endurance limit with increasing notch depth was attributed to the intensified stress concentration at the notch tip,[49] which accelerates crack initiation and propagation under repeated loading. Moreover, HPFRC0 without fibers exhibited early fatigue failure, whereas the embedded fibers in HPFRC1 and HPFRC2 delayed crack propagation by enhancing energy dissipation mechanisms and improving the post-crack

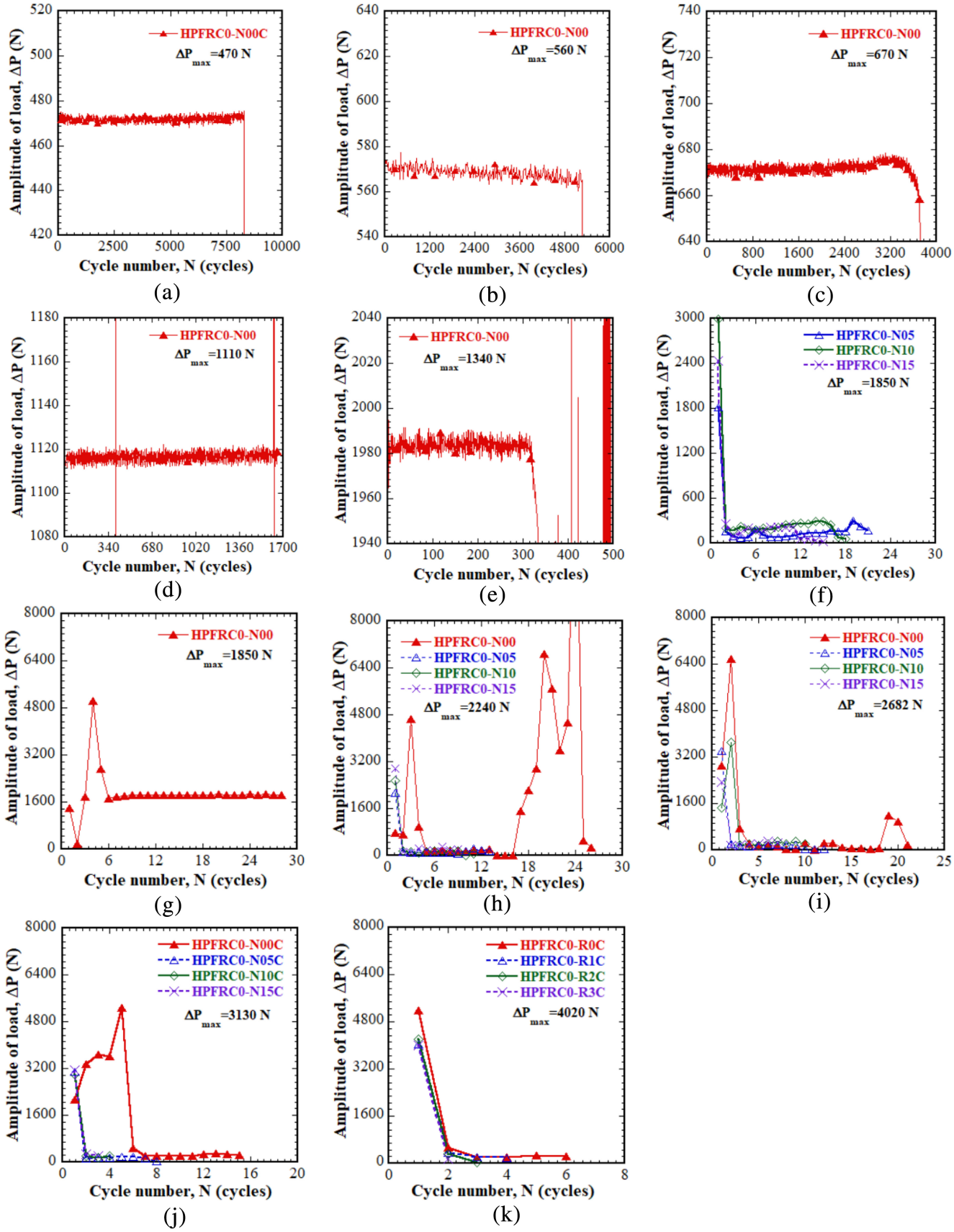


FIGURE 20 Load amplitudes versus cycle numbers response curve of HPFRC0 series. (a) ΔP_{max} = 470 N; (b) ΔP_{max} = 560 N; (c) ΔP_{max} = 670 N; (d) ΔP_{max} = 1110 N; (e) ΔP_{max} = 1340 N; (f) ΔP_{max} = 1850 N; (g) ΔP_{max} = 1850 N; (h) ΔP_{max} = 2240 N; (i) ΔP_{max} = 2682 N; (j) ΔP_{max} = 3130 N; (k) ΔP_{max} = 4020 N.

tensile behavior. This explains the inferior endurance performance under identical loading conditions of HPFRC0.

4.4.2 | Modeling of the fatigue flexural response of HPFRCs

The fatigue curve of $\Delta f_{max} - N$ was performed based on the fatigue model of Basquin[55] using fatigue stress amplitude ($S = \Delta f_{max}$) at Equation (14) and fatigue stress ratio ($S = \Delta f_{max}/f_{MOR}$) at Equation (15).

$$(\Delta f_{max})^p = \frac{C}{N}, \tag{14}$$

$$\left(\frac{\Delta f_{max}}{f_{MOR}}\right)^p = \frac{C}{(f_{MOR})^p N}. \tag{15}$$

The p and C coefficient of the studied concrete with different α were summarized in Table 8. Figures 23 and 24 graphically show the fatigue response curves using Equations (14) and (15), respectively. Although the shapes of the fatigue response curves between Figures 23 and 24 were similar in general, their orders of N in term of notch depth were different according to HPFRC series. For example, at the same $\Delta f_{max}/f_{MOR} < 0.25$ as shown in Figure 24, the HPFRC0 generated the order of notch depth in term of endurance limit as follows: N05 < N10 < N15 < N00, whereas the HPFRC1 and HPFRC2 created their order of N00 < N15 < N10 < N05. At the high $\Delta f_{max}/f_{MOR} > 0.6$, the HPFRCs generally produced the order of notch depth in term of endurance limit as follows: N15 < N10 < N05 < N00, that is, the endurance limits of the HPFRCs reduced with notch depth. Besides, the HPFRCs may be categorized as high-cycle fatigue materials, because their cycle number changed from 100 to 1,000,000.

Table 9 presents a comparative review of existing numerical studies, demonstrating a consistent trend of HPFRCs: increasing notch depth leads to reductions in flexural load-carrying capacity and fracture toughness, as confirmed by both experimental and numerical investigations. Sadaghian et al.[56] and Jiao et al.[20] also confirmed the effect of notch depth on the flexural strength and fracture energy of HPFRCs, with numerical and AE-based measurements providing strong validation. Similarly, Frediani et al.[57] employed FEM to reproduce load–

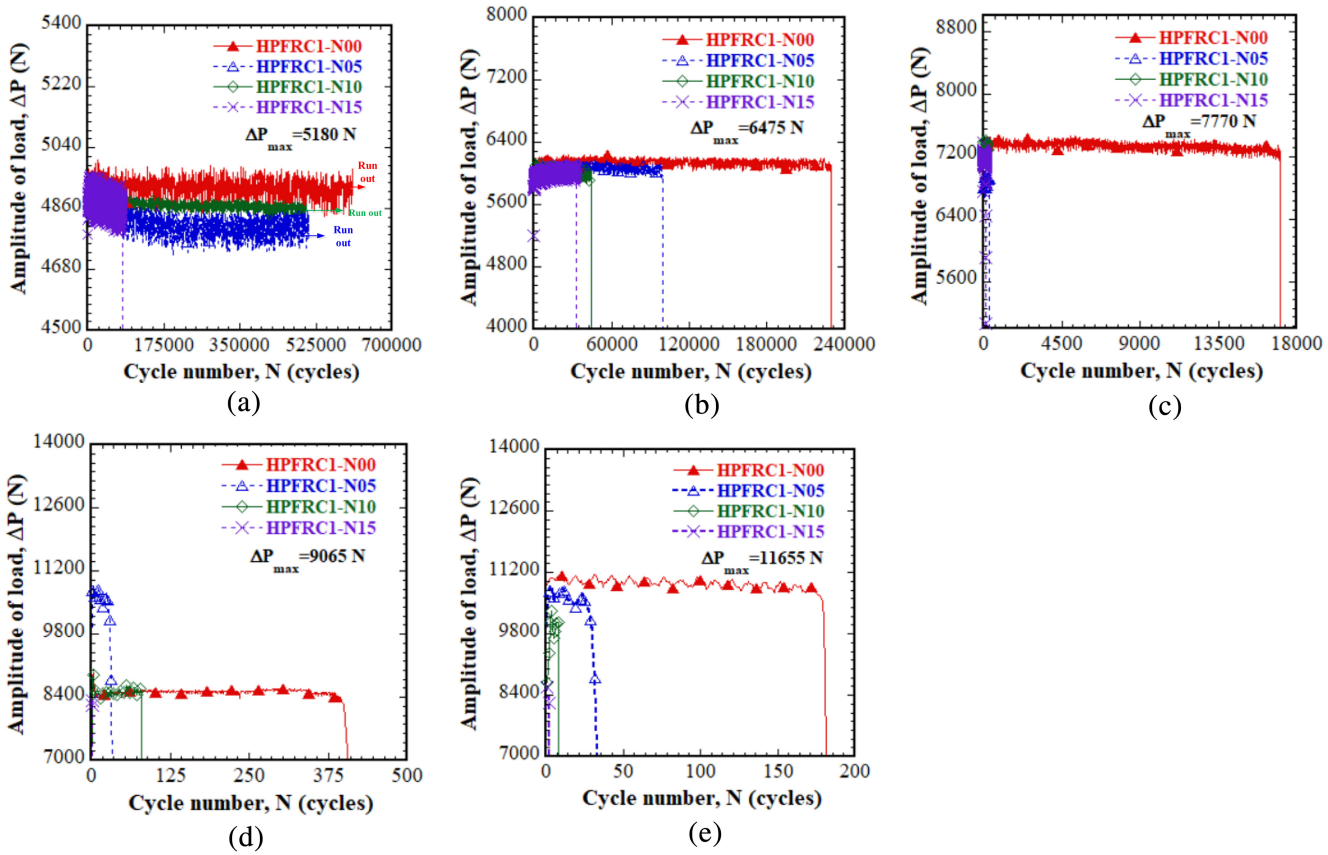


FIGURE 21 Load amplitudes versus cycle numbers response curve of HPFRC1 series. (a) $\Delta P_{max} = 5180$ N; (b) $\Delta P_{max} = 6475$ N; (c) $\Delta P_{max} = 7770$ N; (d) $\Delta P_{max} = 9065$ N; (e) $\Delta P_{max} = 11{,}655$ N.

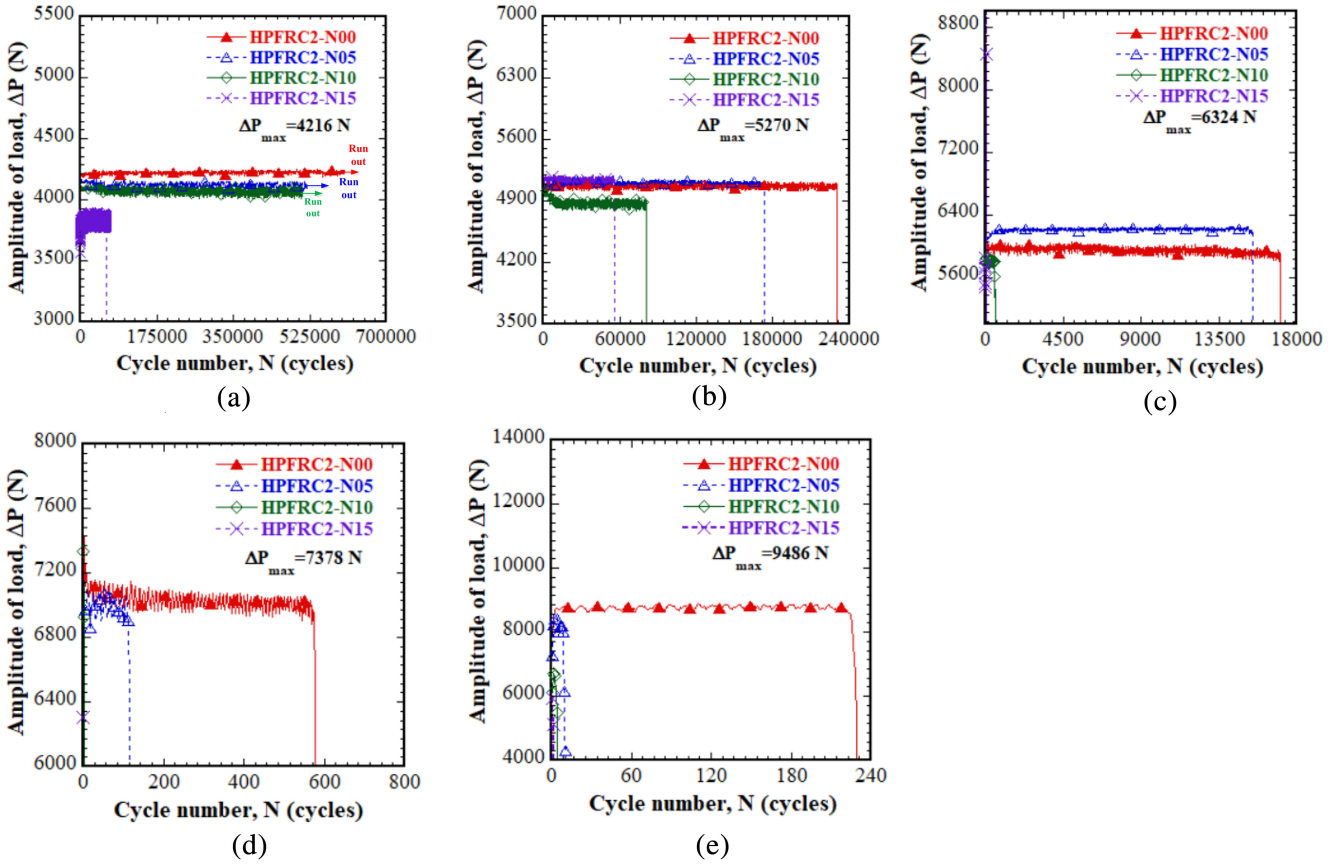


FIGURE 22 Load amplitudes versus cycle numbers response curve of HPFRC2 series. (a) $\Delta P_{max} = 4216$ N; (b) $\Delta P_{max} = 5270$ N; (c) $\Delta P_{max} = 6324$ N; (d) $\Delta P_{max} = 7378$ N; (e) $\Delta P_{max} = 4020$ N.

TABLE 8 Fatigue equations of the HPFRCs regarding stress amplitude.

HPFRC series	Test series	Coefficient *m*	Coefficients *C*	Fatigue equation (14)	Fatigue equation (15)
HPFRC0 series	HPFRC0-N00 [34]	3.68	35493	$(\Delta f_{max})^{3.68} = \frac{35,493}{N}$	$\left(\frac{\Delta f_{max}}{f_{MOR}}\right)^{3.68} = \frac{3.16}{N}$
	HPFRC0-N05	1.60	270	$(\Delta f_{max})^{1.60} = \frac{270}{N}$	$\left(\frac{\Delta f_{max}}{f_{MOR}}\right)^{1.60} = \frac{4.73}{N}$
	HPFRC0-N10	2.42	967	$(\Delta f_{max})^{2.42} = \frac{967}{N}$	$\left(\frac{\Delta f_{max}}{f_{MOR}}\right)^{2.42} = \frac{2.11}{N}$
	HPFRC0-N15	2.68	1228	$(\Delta f_{max})^{2.68} = \frac{1228}{N}$	$\left(\frac{\Delta f_{max}}{f_{MOR}}\right)^{2.68} = \frac{1.39}{N}$
HPFRC1 series	HPFRC1-N00	12.81	7.82×10^{20}	$(\Delta f_{max})^{12.81} = \frac{7.82\times10^{20}}{N}$	$\left(\frac{\Delta f_{max}}{f_{MOR}}\right)^{12.81} = \frac{11.33}{N}$
	HPFRC1-N05	16.88	2.55×10^{25}	$(\Delta f_{max})^{16.88} = \frac{2.55\times10^{25}}{N}$	$\left(\frac{\Delta f_{max}}{f_{MOR}}\right)^{16.88} = \frac{0.18}{N}$
	HPFRC1-N10	16.85	1.74×10^{25}	$(\Delta f_{max})^{16.85} = \frac{1.74\times10^{25}}{N}$	$\left(\frac{\Delta f_{max}}{f_{MOR}}\right)^{16.85} = \frac{0.14}{N}$
	HPFRC1-N15	16.51	1.99×10^{24}	$(\Delta f_{max})^{16.51} = \frac{1.99\times10^{24}}{N}$	$\left(\frac{\Delta f_{max}}{f_{MOR}}\right)^{16.51} = \frac{0.05}{N}$
HPFRC2 series	HPFRC2-N00	12.26	3.27×10^{19}	$(\Delta f_{max})^{12.26} = \frac{3.27\times10^{19}}{N}$	$\left(\frac{\Delta f_{max}}{f_{MOR}}\right)^{12.26} = \frac{17.31}{N}$
	HPFRC2-N05	18.31	8.69×10^{26}	$(\Delta f_{max})^{18.31} = \frac{8.69\times10^{26}}{N}$	$\left(\frac{\Delta f_{max}}{f_{MOR}}\right)^{18.31} = \frac{0.44}{N}$
	HPFRC2-N10	16.83	2.03×10^{24}	$(\Delta f_{max})^{16.83} = \frac{2.03\times10^{24}}{N}$	$\left(\frac{\Delta f_{max}}{f_{MOR}}\right)^{16.83} = \frac{0.17}{N}$
	HPFRC2-N15	16.57	2.47×10^{23}	$(\Delta f_{max})^{16.57} = \frac{2.47\times10^{23}}{N}$	$\left(\frac{\Delta f_{max}}{f_{MOR}}\right)^{16.57} = \frac{0.05}{N}$

displacement behavior, while Khan et al.[58] and Ye et al.[59] reported that increasing notch depth reduces load-carrying capacity. Overall, the results of this study exhibited the same trend as existing numerical works, indicating that the mechanical properties of HPFRCs obtained herein are not unusual. Compared with previous studies, however, the present work provides a more detailed quantification of notch depth effects in HPFRC, covering both static and fatigue loading and distinguishing between different fiber types. A limitation remains in the absence of numerical validation, which is commonly addressed in the reviewed works. Incorporating FEM or probabilistic modeling in future research could enhance the predictive reliability of the experimental findings and enable stronger comparisons with existing literature.

Figure 25 shows a comparison of the flexural fatigue endurance limits for different types of concrete: the HPFRCs from this study, the HPFRC from another publication, high-content hybrid fiber–polymer concrete (HCHFPC),[60] multi-scale cement composite (MSCC),[61] and steel fiber-reinforced concrete (SFRC).[62] The flexural fatigue endurance limits of these composites typically fall within the range of 10^4 to 10^6 cycles; thus, the endurance limits observed for the HPFRCs in this study are consistent with those commonly reported in the literature.

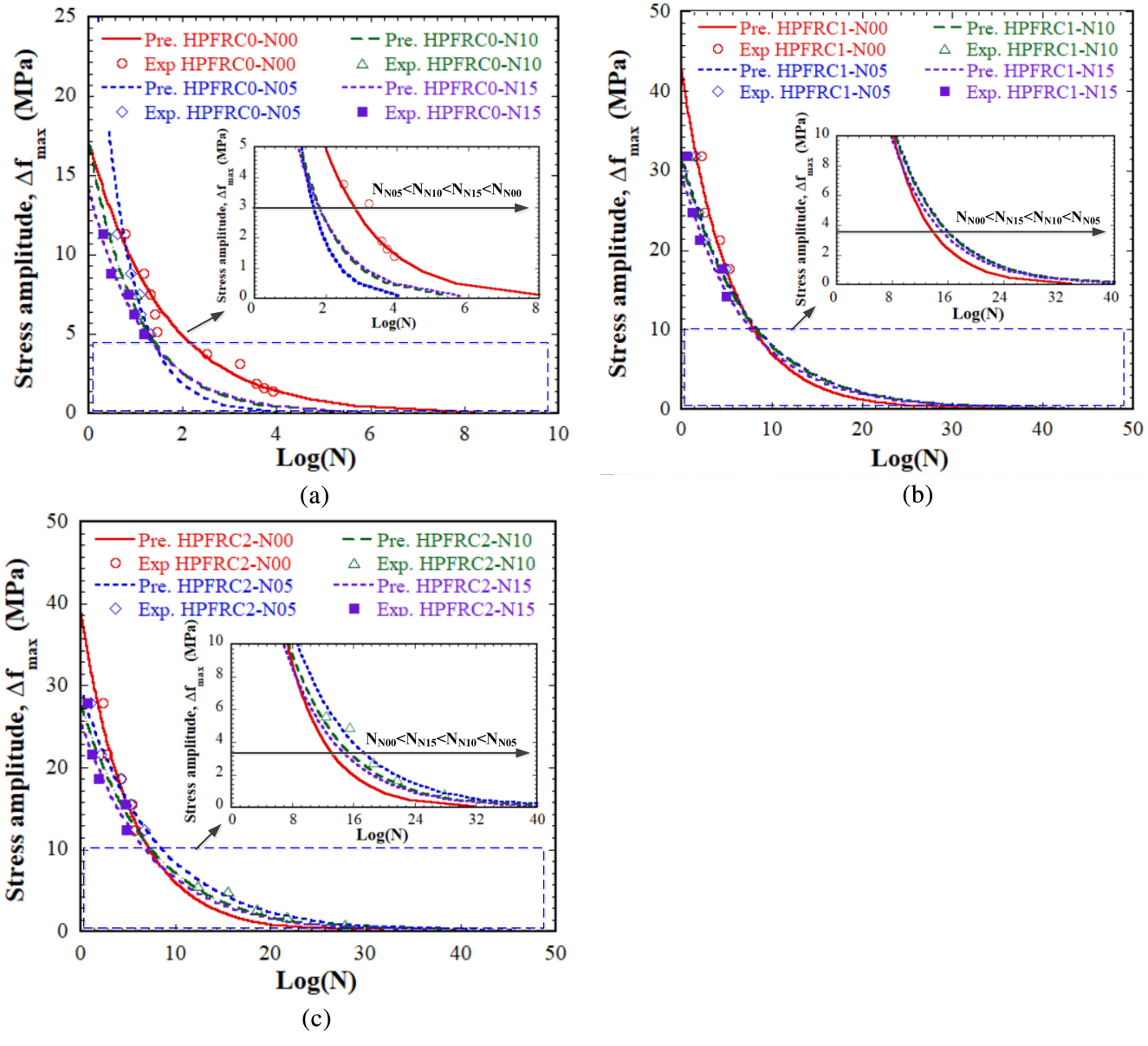


FIGURE 23 Fatigue flexural response of HPFRCs according to stress amplitude. (a) For HPFRC0 series; (b) For HPFRC1 series; (c) For HPFRC2 series.

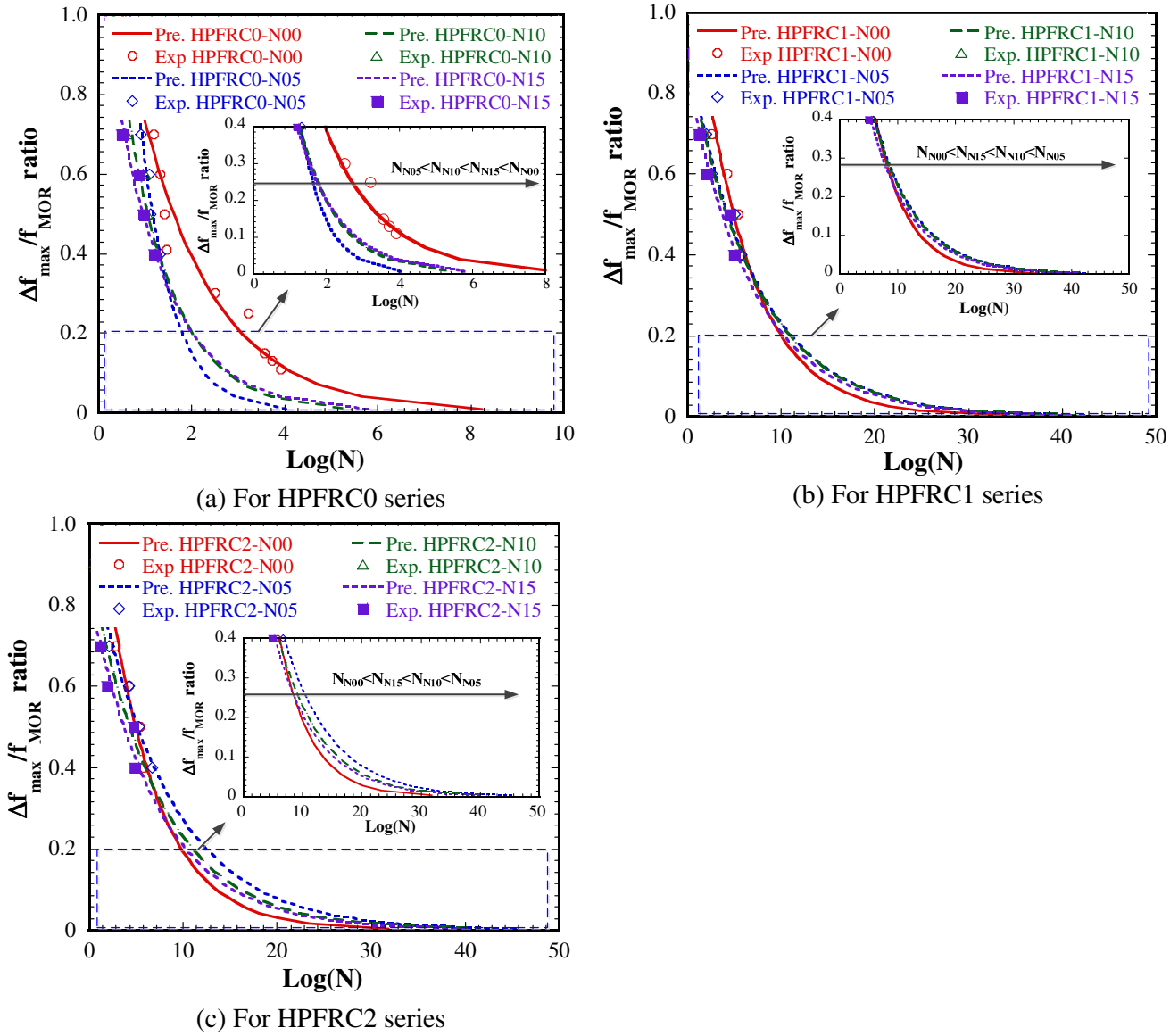


FIGURE 24 Fatigue flexural response of HPFRCs according to stress ratio. (a) For HPFRC0 series; (b) For HPFRC1 series; (c) For HPFRC2 series.

Figure 25b compares the relationship between the stress ratio and the number of cycles (N) for HPFRC with hybrid fiber reinforcement in this study and various types of concrete, including normal concrete[63] and self-compacting concrete.[64] As shown in Figure 25b, the fatigue curve of the HPFRC material in this study lies above those of the other concrete types, indicating a higher fatigue limit compared with that of normal concrete and self-compacting concrete.

5 | CONCLUSIONS

Based on the experimental results and analysis, the following conclusions can be drawn:

- Under static loading, the presence of an initial notch generally reduced the load-carrying and deflection capacities, while slightly increasing the elastic modulus, regardless of HPFRC type. These effects became more pronounced with greater notch depth.
- With increasing notch depth, the flexural strength exhibited an increasing trend for HPFRC0, but decreased for HPFRC1 and HPFRC2.
- As notch depths ranged from 5 to 15 mm under static loading, the HPFRCs exhibited reductions in critical stress intensity factor and critical energy release rate, along with increments in elastic modulus and crack mouth opening displacement. The order of the HPFRC types in terms of flexural resistance was HPFRC0 < HPFRC2 < HPFRC1.

TABLE 9 Different studies with various notch depths alongside key numerical investigations.

References	Material and specimen	Notch (N/D)	Method	Key finding	Comparison
This study	HPFRC, 40 × 40 × 160 mm; span 120 mm	0, 0.125, 0.25, and 0.375	Experiment (3-point bending)	Providing effect of notch depth: increased notch depth reduces load and deflection capacity, K_{IC}, and G_{IC}	Notch depth and hybrid fiber type effecting on flexural responses under static and fatigue loading
Sadaghian et al. (2020) [56]	UHPGC, 40 × 40 × 160 mm	Various N/D (0.2–1.0)	FEM (ATENA)	Observation that specimen notching reduces peak load; a higher N/D ratio increases peak load but decreases residual strength	Confirmation that notch depth reduces strength and toughness of UHPGC; close match between numerical load–CMOD curves and experimental results
Jiao et al. (2023) [20]	UHPGC; 40 × 40 × 160 mm	N/D = 0.2–0.5	Experiment (4-point bending) and AE	Observation that flexural toughness, residual strength, and fracture energy decreased with notch depth; AE energy highly correlated with fracture energy	Close agreement between the present study's observations of reduced flexural and fracture properties of UHPGC with increasing notch depth
Frediani et al. (2024) [57]	HPFRC; 150 × 150 × 600 mm	N/D = 1/6	FEM (mesh refinement)	Observation that FEM accurately reproduces load–displacement curves; response is mesh-size independent; higher fiber content enhances flexural strength of HPFRCs	FEM as a reliable tool for HPFRC flexural analysis, with notch depth and fiber content effects aligning with the present study's results
Khan et al. (2024) [58]	Normal concrete; 100 × 100 × 500 mm	N/D = 0.3	Experiment (3-point bending) and FEM	Observation that ultimate load decreases with increasing notch size, while repair materials effectively restore strength of normal concretes	Confirmation that notch depth reduces the load capacity of normal concretes
Ye et al. (2024) [59]	3D printed ECC; 60–500 mm depth	N/D = 0.23	Experiment (3-point bending) and FEM	Observation that flexural strength decreases with increasing notch depth, fracture toughness varies with specimen size	Providing consistent trends of size and notch effects on the flexural strength of ECC

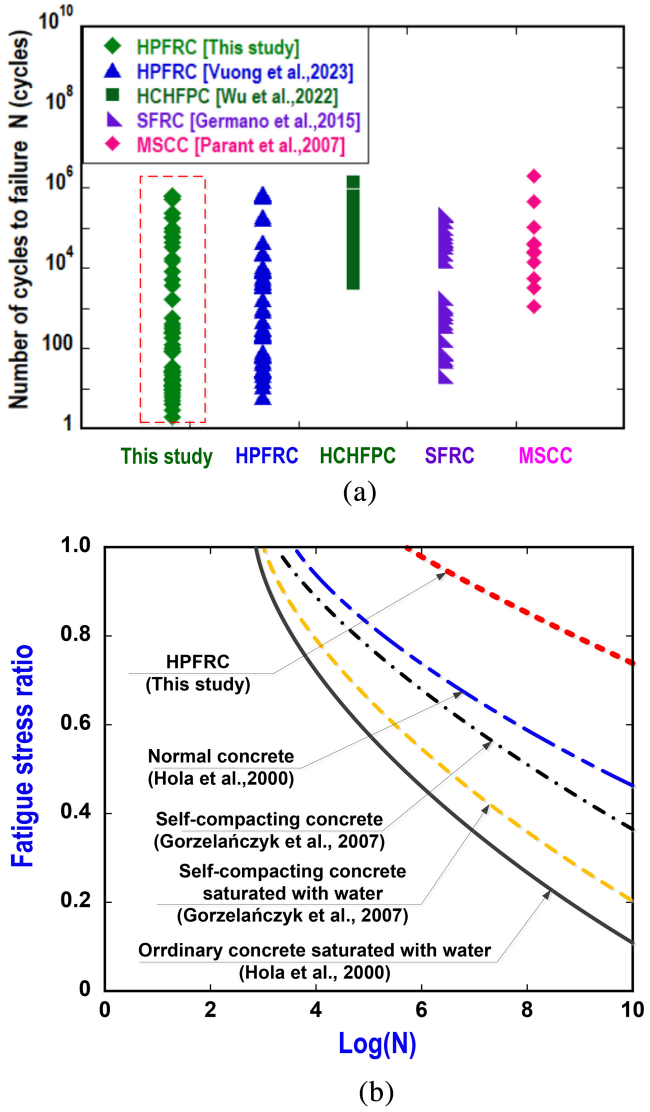


FIGURE 25 Fatigue performance according to various concrete types. (a) Flexural fatigue endurance limits of various concrete types. (b) Fatigue response curves of different concrete types.

- Under fatigue loading with a low $\Delta f_{max}/f_{MOR} < 0.25$, HPFRC0 exhibited an endurance ranking of N05 < N10 < N15 < N00, while HPFRC1 and HPFRC2 showed an endurance order of N00 < N15 < N10 < N05, with respect to notch depth.
- Under fatigue loading with a high $\Delta f_{max}/f_{MOR} > 0.6$, the endurance limits of the HPFRCs generally decreased with increasing notch depth. Overall, the results suggest that HPFRCs can be classified as high-cycle fatigue materials, with fatigue lives ranging from 100 to 1,000,000 cycles.

In this study, the mechanical and fracture behaviors of HPFRCs were investigated using notched specimens subjected to static and cyclic bending. Nevertheless, some limitations should be acknowledged, including the relatively small specimen size and limited number of experiments, which will be progressively addressed in future work.

ACKNOWLEDGMENTS

This research is funded by Vietnam National Foundation for Science and Technology Development (NAFOSTED) under grant number 107.01-2021.69.

CONFLICT OF INTEREST STATEMENT

The authors declare that they have no known competing financial interests or personal relationships that could have appeared to influence the work reported in this paper.

DATA AVAILABILITY STATEMENT

The data that support the findings of this study are available from the corresponding author upon reasonable request.

ORCID

Kha-Ky Lam https://orcid.org/0009-0006-6784-4787

REFERENCES

1. Saladi N, Montanari L, Mohebbi A, Cooper MA, Graybea B. Assessing the setting behavior of ultra-high performance concrete. Mater Struct. 2024;57:143.
2. Abellán-García J, Carvajal-Muñoz JS, Ramírez-Munévar C. Application of ultra-high-performance concrete as bridge pavement overlays: literature review and case studies. Construct Build Mater. 2024;410:134221.
3. El-Abbasy AA. Tensile, flexural, impact strength, and fracture properties of ultra-high-performance fiber-reinforced concrete – a comprehensive review. Construct Build Mater. 2023;408:133621.
4. Tran NT, Nguyen TK, Nguyen DL, Le QH. Assessment of fracture energy of strain-hardening fiber-reinforced cementitious composite using experiment and machine learning technique. Struct Concr. 2023;24(3):4185–98. https://doi.org/10.1002/suco.202200332
5. Nguyen DL, Ngo TT, Phan TD, Lai T-T, Le D-V. Predicting tensile properties of strain-hardening concretes containing hybrid fibers from single fiber pullout resistance. J Sci Technol Civil Eng. 2022;16(3):84–96.
6. Tran TK, Tran NT, Kim DJ. Enhancing impact resistance of hybrid ultra-high-performance fiber-reinforced concretes through strategic use of polyamide fibers. Construct Build Mater. 2021;271:121562.
7. Cheng J, Fu C, Chen Z, Zhu X, Ye H. Intrinsic self-sensing piezoresistive behaviors of ultra-high strength alkali-activated concrete. J Build Eng. 2024;96:110644. https://doi.org/10.1016/j.jobe.2024.110644
8. Elseady AAE, Zhuge Y, Ma X, Chow CWK, Lee I, Zeng J, et al. Development of self-sensing cementitious composites by

incorporating a two-dimensional carbon-fibre textile network for structural health monitoring. Construct Build Mater. 2024; 415:135049. https://doi.org/10.1016/j.conbuildmat.2024.135049
9. Lee SH, Kim JH, Han SJ, Yi ST, Kim KS. Self-sensing capability of ultra-high performance fiber-reinforced concrete with multi-walled carbon nanotubes. J Build Eng. 2024;86:108972. https://doi.org/10.1016/j.jobe.2024.108972
10. Nguyen DL, Lam MN-T, Kim DJ, Song J. Direct tensile self-sensing and fracture energy of steel-fiber-reinforced concretes. Compos Part B Eng. 2020;183:107714. https://doi.org/10.1016/j.compositesb.2019.107714
11. Walraven J, Droogné D, Grünewald S, Taerwe L, Cotovanu B, Rovers J. Self-compacting high-performance fiber concrete for foundations: part 1 – experimental verification and design considerations. Struct Concr. 2022;23:172–86. https://doi.org/10.1002/suco.202000440
12. Abdolpour H, Niewiadomski P, Sadowski L, Kwiecień A. Engineering of ultra-high performance self-compacting mortar with recycled steel fibres extracted from waste tires. Arch Civ Mech Eng. 2022;22:175. https://doi.org/10.1007/s43452-022-00496-4
13. Yao C, Shen A, Guo Y, Lyu Z, He Z, Wu H. A review on autogenous self-healing behavior of ultra-high performance fiber reinforced concrete (UHPFRC). Arch Civil Mech Eng. 2022; 22(3):145.
14. Xi B, Ferrara L. Evolution of self-healing performance of UHPC exposed to aggressive environments and cracking/healing cycles. Mater Struct. 2024;57:36. https://doi.org/10.1617/s11527-024-02312-2
15. Doostkami H, Roig-Flores M, Serna P. Self-healing efficiency of ultra high-performance fiber-reinforced concrete through permeability to chlorides. Construct Build Mater. 2021;310:125168. https://doi.org/10.1016/j.conbuildmat.2021.125168
16. Niu Y, Wei J, Jiao CJC. Crack propagation behavior of ultra-high-performance concrete (UHPC) reinforced with hybrid steel fibers under flexural loading. Dent Mater. 2021;294:123510.
17. Askar MK, Al-Kamaki Y, Ferhadi R, Majeed HK. Cracks in concrete structures causes and treatments: a review. J Duhok Univ. 2023;26(2):148–65.
18. Li Z, Gong Y, Chen F. Simulation of mixed mode I-II crack propagation in concrete using toughness-based crack initiation-propagation criterion with modified fracture energy. Theor Appl Fract Mech. 2023;123:103701. https://doi.org/10.1016/j.tafmec.2022.103701
19. Hou Z, Yuan R, Chen Y, Sun W. Crack propagation process in double-flawed granite under compression using digital image correlation method and numerical simulation. Sci Rep. 2024; 14:21424. https://doi.org/10.1038/s41598-024-72302-5
20. Jiao Y, Fang M, Han X, Yang H. Effect of notch-to-depth ratio on flexural and fracture behaviors of UHPGC notched beams based on four-point bending test and acoustic emission. Eng Fract Mech. 2023;290:109524.
21. Yin YQ, Hu SW. Four-point bending tests for the fracture properties of concrete. Eng Fract Mech. 2019;211:371–81.
22. Qin S, Gao D, Wang Z, Zhu H. Research on the fracture behavior of steel-fiber-reinforced high-strength concrete. Materials. 2022;15(1):135. https://doi.org/10.3390/ma15010135
23. Vandecruys E, De Smedt M, Vrijdaghs R, Verstrynge E, Vandewalle L. Sectional analysis of the cyclic behavior of steel fiber reinforced concrete. Struct Concr. 2021;22(5):3123–39. https://doi.org/10.1002/suco.202000763
24. Zhu L, Li T, Wang Y, Tang Q, Wang G, Zhang Z. Experimental and numerical study on T-shaped UHPFRC beams with high-strength reinforcement. Struct Concr. 2021;22(6):3630–45.
25. Nasiri H, Pourbaba M, Lotfollahi Yaghin MA. Numerical study on the flexural and shear behavior of steel fiber and high-strength steel combination in ultra-high-performance fiber-reinforced concrete beams under cyclic loading. Struct Concr. 2025;26(3):3663–77. https://doi.org/10.1002/suco.202300760
26. Lam KK, Nguyen DL, Le MT, Tran NT. Flexural and fracture behavior of high-performance concrete using notch specimen. J Sci Technol Civil Eng. 2024;18(3):102–13.
27. Nguyen DL, Thai DK, Ngo TT, Tran TK, Nguyen TT. Weibull modulus from size effect of high-performance fiber-reinforced concrete under compression and flexure. Construct Build Mater. 2019;226:743–58.
28. Vuong TNH, Nguyen DL, Nguyen HT, Nguyen TNM. Effect of fiber content on flexural fracture parameters of high-performance steel fiber-reinforced concrete. J Sci Technol Civil Eng. 2024;18(1):12–23.
29. Nguyen DL, Thai DK, Nguyen HT, Tran NT, Phan TD, Kim DJ. Mechanical behaviors and their correlations of ultra-high-performance fiber-reinforced concretes with various steel fiber types. Struct Concr. 2023;24(1):1179–200.
30. Htet P, Chen W, Huang Z, Hao H. Physical and mechanical properties of deflection-hardening hybrid fibre-reinforced recycled aggregate concrete. J Build Eng. 2024;90:109510.
31. Park JJ, Yoo DY, Park GJ, Kim SW. Feasibility of reducing the fiber content in ultra-high-performance fiber-reinforced concrete under flexure. Materials. 2017;10:118.
32. Nguyen DL, Lam KK, Le VB, Tran MP. A predictive model for modulus of rupture of hybrid fiber-reinforced concrete from fiber-matrix bond resistance. Transp Res Procedia. 2025;85:2–9.
33. Nguyen DL, Le HV, Vu TBN, Nguyen VT, Tran NT. Evaluating fracture characteristics of ultra-high-performance fiber-reinforced concrete in flexure and tension with size impact. Construct Build Mater. 2023;382:131224.
34. Kim DJ, Park SH, Ryu GS, Koh KT. Comparative flexural behavior of hybrid ultra-high performance fiber reinforced concrete with different macro fibers. Construct Build Mater. 2011; 25(11):4144–55.
35. Nguyen DL, Thai DK, Kim DJ. Direct tension-dependent flexural behavior of ultra-high-performance fiber-reinforced concretes. J Strain Anal Eng Des. 2017;52(2):121–34.
36. Kosa K, Naaman A, Hansen W. Durability of fiber reinforced mortar. ACI Mater J. 1991;88(3):310–9.
37. Wöhler A. Über die festigkeitsversuche mit eisen und stahl. Berlin, Germany: Ernst & Korn; 1870.
38. Nguyen DL, Thai DK, Lam MNT. Synergy in flexure of high-performance fiber-reinforced concrete with hybrid steel fibers. J Mater Civ Eng. 2022;34(6):04022090.
39. Vuong TNH, Nguyen TK, Nguyen DL, Le HV, Tran NT. Fiber fraction-dependent flexural behavior of high-performance fiber-reinforced concrete under static and repeated loading. J Build Eng. 2023;79:107808.
40. Bai Y, Jin WL. Chapter 25—Fatigue capacity. Marine structural design. 2nd ed. Oxford, UK: Butterworth-Heinemann; 2016. p. 489–507.
41. Ballinger CA. Cumulative fatigue damage characteristics of plain concrete. Highway Res Rec. 1971;370:1–11.

42. Kesler CE. Effect of speed of testing on flexural fatigue strength of plain concrete. Proceedings of the highway research board. Volume 32. Washington, D.C., USA: Highway Research Board; 1953. p. 251–8.
43. BS 7608:1993. Code of practice for fatigue design and assessment of steel structures. London, UK: British Standards Institution; 1993.
44. Hsu TT. Fatigue of plain concrete. J. Proc. 1981;78(4):292–305.
45. Gao S, Qi L, Zhu Y, Wang W. Effect of notch depth ratio on mode I and mixed mode I-II fracture properties of engineered cementitious composites (ECC). Int J Solids Struct. 2022;236:111363.
46. Deng Y, Zhang Z, Shi C, Wu Z, Zhang C. Steel fiber–matrix interfacial bond in ultra-high-performance concrete: a review. Engineering. 2023;22:215–32.
47. ASTM D5045-14. Standard test methods for plane-strain fracture toughness and strain energy release rate of plastic materials. Conshohocken, Pennsylvania, United States: ASTM International; 2022.
48. Chaudhari TS, Mathews NG, Mishra AK, Sahasrabuddhe HP, Jaya BN. Energy release rate formulations for non-conventional fracture test geometries. JOM. 2021;73:1597–606.
49. Vuong TNH, Nguyen TK, Nguyen DL, Thai D-K, Tran N-T. Static and cyclic behavior of high-performance concrete reinforced with hybrid steel fibers using notched and un-notched flexural specimen. Construct Build Mater. 2024;449:138430.
50. Liu J, Zang S, Yang F, Zhang M, Li A. Fracture mechanical properties of steel fiber reinforced self-compacting concrete under dry–wet cycle sulfate attack. Buildings. 2022;12(10):1623. https://doi.org/10.3390/buildings12101623
51. Han J, Huang D, Chen J, Lan X. Experiment study and finite element analysis of the coupling effect of steel fiber length and coarse aggregate maximum size on the fracture properties of concrete. Crystals. 2021;11(8):850.
52. Dong W, Wu Z, Zhou X, Wang C. A comparative study on two stress intensity factor-based criteria for prediction of mode-I crack propagation in concrete. Eng Fract Mech. 2016;158:39–58. https://doi.org/10.1016/j.engfracmech.2016.02
53. Park SH, Kim DJ, Ryu GS, Koh KT. Tensile behavior of ultra-high-performance hybrid fiber reinforced concrete. Construct Build Mater. 2012;34(2):172–84.
54. Guinea GV, Pastor JY, Planas J, Elices M. Stress intensity factor, compliance and CMOD for a general three-point-bend beam. Int J Fract. 1998;89:103–16.
55. Oh, B. H. The exponential law of endurance tests. In Proceedings of the American Society for Testing and Materials(Vol. 70, pp. 625–30). ASTM International, Conshohocken, Pennsylvania, United States, 1970.
56. Sadaghian H, Pourbaba M, Andabili SZ, Mirmiran A. Experimental and numerical study of flexural properties in UHPFRC beams with and without an initial notch. Construct Build Mater. 2021;268:121196.
57. Matías F, Martín A, Bibiana L. Reinforcement of Concrete Structures with High-Performance Fiber-reinforced Concrete (HPFRC). J. Build. Eng. 2024;6(2):93–104. https://doi.org/10.32629/jbt.v6i2.2547
58. Khan W, Akhtar S, Rawat A, Basu A. Experimental and numerical study on flexural behavior of concrete beams using notches and repair materials. Sustainability. 2024;16:2723. https://doi.org/10.3390/su16072723
59. Ye J, Yang M, Yu J, Dai Y, Yin BB, Weng Y. Size effect on flexural and fracture behaviors of 3D printed engineered cementitious composites: experimental and numerical studies. Eng Struct. 2024;298:117062.
60. Banjara NK, Ramanjaneyulu K, Sasmal S. Flexural fatigue performance of plain and fiber reinforced concrete. Trans Indian Inst Met. 2016;69:373–7. https://doi.org/10.1007/s12666-015-0770-y
61. Parant E, Rossi P, Boulay C. Fatigue behavior of a multi-scale composite. Cem Concr Res. 2007;37:264–9. https://doi.org/10.1016/j.cemconres.2006.04.006
62. Germano F, Tiberti G, Plizzari G. Post-peak fatigue performance of steel fiber reinforced concrete under flexure. Mater Struct. 2015;49(10):4229–45. https://doi.org/10.1617/s11527-015-0783-3
63. Hoła J. Initiating and critical stresses and stress failure in concrete under compression. Sci Pap Inst Build Eng Wrocław Univ Technol. 2000;76(33):182.
64. Gorzelanczyk T, Hoła J. Assessment of the failure of self-compacting concretes differing in their air pore structure by acoustic techniques. Defektoskopie 2007: 37th International Conference and Exhibition, European NDT Days in Prague November 2007; 2008. https://www.ndt.net/?id=5510

AUTHOR BIOGRAPHIES



Kha-Ky Lam, Research Assistant, Faculty of Civil Engineering, Ho Chi Minh City University of Technology and Education, No. 01 Vo Van Ngan St, Thu Duc Ward, Ho Chi Minh City, Vietnam. Email: khaky0103@gmail.com.



Duy-Liem Nguyen, Associate Professor, PhD, Faculty of Civil Engineering, Ho Chi Minh City University of Technology and Education, No. 01 Vo Van Ngan St, Thu Duc Ward, Ho Chi Minh City, Vietnam. Email: liemnd@hcmute.edu.vn.



H. T. Tai Nguyen, PhD, Faculty of Civil Engineering, Ho Chi Minh City University of Technology and Education, No. 01 Vo Van Ngan St, Thu Duc Ward, Ho Chi Minh City, Vietnam. Email: tainht@hcmute.edu.vn.



Kien Le-Trung, PhD, Faculty of Civil Engineering, Ho Chi Minh City University of Technology and Education, No. 01 Vo Van Ngan St, Thu Duc Ward, Ho Chi Minh City, Vietnam. Email: kienlt@hcmute.edu.vn.



Ngoc-Thanh Tran, Associate Professor, PhD, Institute of Civil Engineering, Ho Chi Minh City University of Transport, No. 02 Vo Oanh St, Thanh My Tay Ward, Ho Chi Minh City, Vietnam. Email: ngocthanh.tran@ut.edu.vn.



Huy-Viet Le, Lecturer, PhD, Faculty of Civil Engineering, Hanoi University of Mining and Geology, No. 18 Vien Street, Dong Ngac Ward, Ha Noi, Vietnam. Email: lehuyviet@humg.edu.vn.

How to cite this article: Lam K-K, Nguyen D-L, Nguyen HTT, Le-Trung K, Tran N-T, Le H-V. Notch depth-dependent flexural behavior of high-performance fiber-reinforced concrete under static and cyclic loading. Structural Concrete. 2026;27(2): 2621–55. https://doi.org/10.1002/suco.70365